HHS Public Access

Author manuscript

Cell Rep. Author manuscript; available in PMC 2024 September 22.

Published in final edited form as:

Cell Rep. 2024 August 27; 43(8): 114506. doi:10.1016/j.celrep.2024.114506.

Transcriptional programming mediated by the histone demethylase KDM5C regulates dendritic cell population heterogeneity and function

Hannah Guak[1,2,8], **Matthew Weiland**[1,8], **Alexandra Vander Ark**[1], **Lukai Zhai**[1], **Kin Lau**[3], **Mario Corrado**[1,4], **Paula Davidson**[1], **Ebenezer Asiedu**[1], **Batsirai Mabvakure**[1,5,6], **Shelby Compton**[1], **Lisa DeCamp**[1], **Catherine A. Scullion**[1,7], **Russell G. Jones**[1], **Sara M. Nowinski**[1], **Connie M. Krawczyk**[1,9,*]

[1]Department of Metabolism and Nutritional Programming, Van Andel Institute, Grand Rapids, MI 49503, USA

[2]Department of Pediatrics, University of Michigan, Ann Arbor, MI 48109, USA

[3]Bioinformatics and Biostatistics Core, Van Andel Institute, Grand Rapids, MI 49503, USA

[4]Department of Internal Medicine, University of Toronto, Toronto, ON M5S 3H2, Canada

[5]Department of Oncology, Georgetown University School of Medicine, Washington, DC 20057, USA

[6]Georgetown Lombardi Comprehensive Cancer Center, Georgetown University, Washington, DC 20057, USA

[7]Department of Experimental Medicine, Dana-Farber Cancer Institute, Boston, MA 02215, USA

[8]These authors contributed equally

[9]Lead contact

SUMMARY

Functional and phenotypic heterogeneity of dendritic cells (DCs) play crucial roles in facilitating the development of diverse immune responses essential for host protection. Here, we report that KDM5C, a histone lysine demethylase, regulates conventional or classical DC (cDC) and plasmacytoid DC (pDC) population heterogeneity and function. Mice deficient in KDM5C in DCs have increased proportions of cDC2Bs and cDC1s, which is partly dependent on type I interferon (IFN) and pDCs. Loss of KDM5C results in an increase in Ly6C^{-} pDCs, which, compared

*Correspondence: connie.krawczyk@vai.org.

AUTHOR CONTRIBUTIONS

H.G., M.W., C.M.K., L.Z., and S.M.N. wrote and edited the manuscript. H.G., M.W., A.V.A., L.Z., M.C., P.D., S.C., L.D., E.A., and C.S. performed experiments. K.L. and B.M. performed bioinformatic analyses. H.G., M.W., A.V.A., L.Z., K.L., M.C., P.D., R.G.J., S.M.N., and C.M.K. provided intellectual contributions and project support. C.M.K., H.G., and M.W. managed the project.

SUPPLEMENTAL INFORMATION

Supplemental information can be found online at https://doi.org/10.1016/j.celrep.2024.114506.

DECLARATION OF INTERESTS

The authors declare no competing interests.

to Ly6C$^+$ pDCs, have limited ability to produce type I IFN and more efficiently stimulate antigen-specific CD8 T cells. KDM5C-deficient DCs have increased expression of inflammatory genes, altered expression of lineage-specific genes, and decreased function. In response to *Listeria* infection, KDM5C-deficient mice mount reduced CD8 T cell responses due to decreased antigen presentation by cDC1s. Thus, KDM5C is a key regulator of DC heterogeneity and critical driver of the functional properties of DCs.

Graphical Abstract

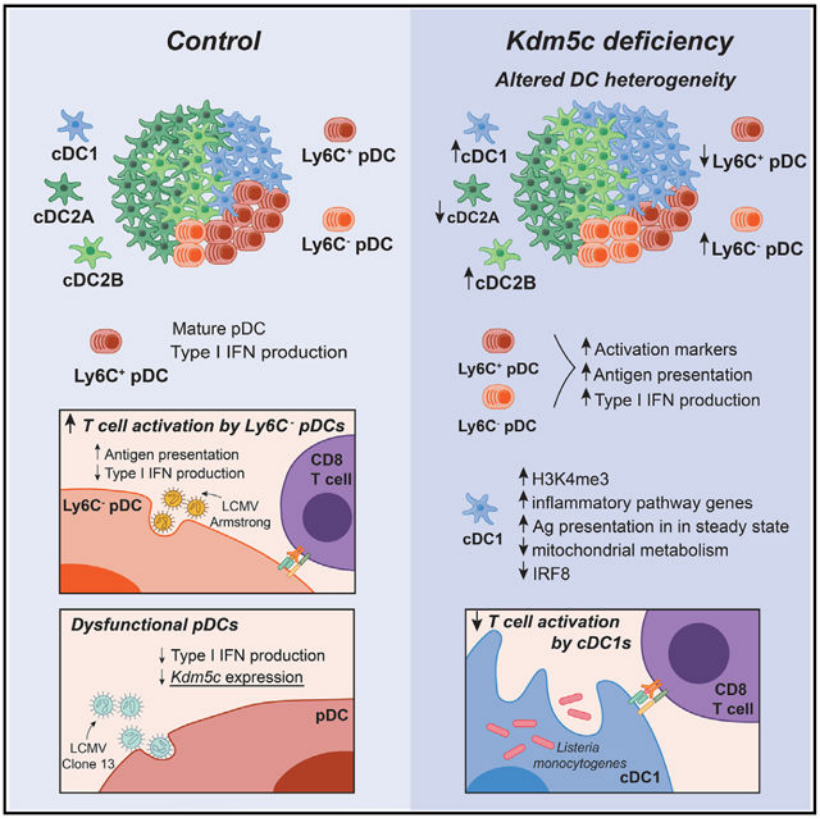

In brief

Guak et al. report that the histone lysine demethylase KDM5C fine-tunes lineage-specific gene expression and regulates the composition of DC populations. Loss of KDM5C leads to increased IRF-driven inflammatory gene expression at steady state, resulting in diminished type I IFN production and antigen presentation when stimulated.

INTRODUCTION

Dendritic cells (DCs) are innate immune cells that play key roles in shaping innate and adaptive immunity. Like many immune cell types, DCs are a heterogeneous population comprising subsets that are classified based on ontogeny, transcriptional signatures, and functional properties.[1–3] Their functional and phenotypic heterogeneity enables them to orchestrate customized immune responses that afford host protection against

a diverse range of threats. Conventional or classical DCs (cDCs) are myeloid-derived and are functionally divided into two major subsets: cDC1 ($CD8^+XCR1^+$) and cDC2 ($CD4^+CD172a^+CD11b^+$). cDC2 can be further divided into cDC2A ($ESAM^+CLEC12A^-$) and cDC2B ($ESAM^-CLEC12A^+$), which are also defined by the expression of the transcription factors (TFs) T-BET and RORγt, respectively.[4] cDCs are exceptionally efficient at presenting antigen to T cells, with cDC1s being specialized to cross-present antigens and stimulate CD8 T cell responses that are known for their cytolytic activity. cDC2As are considered more regulatory, whereas cDC2B are relatively more inflammatory.[4] Both cDC2A and cDC2B are known to promote CD4 T cell responses, which shape the nature of immune responses. cDC subsets are generally thought to arise from a common pool of pre-DCs that are committed to preferentially differentiate into cDC1 or cDC2.[5,6] However, more recently, plasmacytoid DC (pDC)-like cells have been shown to give rise to cDC2 populations.[7]

pDCs are another class of DC that can participate in T cell priming in certain contexts, but they are primarily known for their capacity to produce large amounts of type I interferons (IFNs). Although less phenotypic heterogeneity has been described for pDCs, there is increased evidence of heterogeneity in the pDC population.[8–10] In addition, pDC-like cells that possess characteristics of both pDCs and cDCs have been described in mice and humans.[7,11–14] These cells have transcriptional profiles associated with pDCs but are poor producers of type I IFN and have an increased capacity for antigen presentation. Recent studies using single-cell RNA sequencing (RNA-seq) to better delineate DC ontogeny have shown that pDCs are predominantly lymphoid in origin, although the precise contribution from the myeloid lineage is still debated.[8,15,16] In fact, one recent study suggests that pDCs and cDC1s have a common precursor that is distinct from cDC2 precursors.[16] Thus, the origins and differentiation trajectory of pDCs are still actively being defined, along with the mechanisms that guide DC fate.

Several TFs have been identified that support epigenetic and transcriptional programming controlling DC specification.[4,17–19] Deletion of these factors leads to either decreased production of a specific DC subset and/or a DC subset with abnormal identity.[20–23] IFN regulatory factor (IRF) 8 and IRF4 promote lineage specificity and function of pDCs and cDCs. IRF8 is required for the development of cDC1s, as well as for the maintenance of cDC1 identity once differentiated.[24] Although IRF8 is not required for pDC differentiation, it is essential for pDC function, including for type I IFN production.[24] In contrast, IRF4 is not required for cDC1 or pDC differentiation and function, but supports those of cDC2s.[20,25] The amount of IRF8 or IRF4 is key for cDC identity, as high amounts of IRF8 are required for cDC1 identity, and a high abundance of IRF4 can induce a similar transcriptional program, including the majority of cDC1-specific genes.[26]

While significant advancements in involvement of TFs in DC specification and function have been made, the roles of chromatin modifiers in these processes is less well understood. Chromatin modifiers play a crucial role in modulating gene expression by modifying the chromatin state (active, poised, repressed) through deposition and removal of histone post translational modifications. The histone lysine demethylase KDM5C (SMCX, JARID1C) is a chromatin-modifying enzyme that removes permissive methyl groups from histone H3K4,

thereby acting as a transcriptional repressor.[27] However, it is well established that KDM5C can promote gene expression in certain contexts.[28,29] KDM5C has largely been studied in the settings of neurodevelopment and cancer. While a function for KDM5C in immune cells has not been described *in vivo*, KDM5C has been shown to regulate immune genes in non-immune cell types.[30–33]

We previously showed that PCGF6, a polycomb protein found in complex with KDM5C, can restrain the inflammatory phenotype of bone marrow-derived DCs (BMDCs) *in vitro*. This phenotype is in part dependent on KDM5C, which was the first evidence that KDM5C is an important regulator of immune cell function.[34] To understand the function of KDM5C in DCs *in vivo*, we generated mice deficient in KDM5C in DCs ($Kdm5c^{\Delta Itgax}$ and $Kdm5c^{\Delta Zbtb46}$). Surprisingly, we found that the composition of DC subsets was altered in the absence of KDM5C. We found that $Kdm5c^{\Delta Itgax}$ mice display a specific increased proportion of cDC1 compared with cDC2, accompanied by an imbalance in cDC2 subsets, with a marked increase in cDC2Bs and decrease in cDC2A. Additionally, $Kdm5c^{\Delta Itgax}$ mice have an increase in $Ly6C^-$ pDCs, which we found are poor producers of type I IFN, but have enhanced capabilities to stimulate antigen-specific CD8 T cells. Both KDM5C-deficient $Ly6C^-$ and $Ly6C^+$ pDCs are more activated but impaired in producing type I IFN. This phenotype is consistent with exhausted pDCs generated during chronic infection, in which we find decreased *Kdm5c* expression.

Mechanistically, we find that KDM5C regulates epigenetic and transcriptional programming, as KDM5C deficiency leads to enhanced expression of inflammatory genes, despite decreased DC function. KDM5C specifically regulates the IRF signaling node, as several IRF TFs show altered gene expression and the balance of IRF4 and IRF8 expression is skewed. In KDM5C-deficient cDC1, the expression of cDC1 lineage-specific genes including *Irf8* was decreased, whereas cDC2 lineage genes were increased. $Kdm5c^{\Delta Itgax}$ mice had reduced CD8 T cell responses to *Listeria* infection due to decreased antigen presentation ability of cDC1s, demonstrating the requirement of KDM5C for cDC1 function. Together, our data show that the histone lysine demethylase KDM5C uniquely functions in DCs to regulate DC specificity and function.

RESULTS

KDM5C regulates DC population heterogeneity

To investigate the function of KDM5C in DCs *in vivo*, we generated mice with KDM5C deficiency in pDCs and cDCs (*Itgax-Cre-*$Kdm5c^{fl/fl}$; $Kdm5c^{\Delta Itgax}$) and examined the abundance and proportions of DC populations in the spleen (Figures 1, S1A, and S1B). The loss of KDM5C did not have a significant impact on the number of cDCs ($Lineage^-CD64^-MHCII^+CD11c^+CD26^+$) but significantly altered the composition of this population (Figure 1A). The proportion of cDC1s ($XCR1^+$), cDC2Bs ($CD172a^+ESAM^-CLEC12A^+$), and merocytic DCs ($XCR1^-CD172a^-$) were higher in $Kdm5c^{\Delta Itgax}$ mice compared with control mice (Figure 1A), whereas cDC2As ($ESAM^+CLEC12A^-$) were lower.[4,9,35,36] Total counts were different for only cDC2A and cDC2B (Figure S1B).

Cre expression under the control of the *Cd11c* promoter is not exclusive to cDCs and also includes expression in pDCs, along with some macrophages[37]; therefore, to examine the effects of KDM5C deletion specifically in cDCs, we generated mice with KDM5C deleted in ZBTB46-expressing cells ($Kdm5c^{\Delta Zbtb46}$). Comparison of cDC1 versus cDC2 populations in $Kdm5c^{\Delta Zbtb46}$ mice showed similar trends as $Kdm5c^{\Delta Itgax}$ mice (Figure S1C); however, the magnitude was less than that observed in the $Kdm5c^{\Delta Itgax}$ mice. Further, cDC2A and cDC2B proportions were not affected by *Kdm5c* deletion in $Kdm5c^{\Delta Zbtb46}$ mice (Figure S1C). There are several possibilities as to why these two models differ. *Itgax-Cre* and *Zbtb46-Cre* are both expressed in the pre-cDC stage[37]; however, the relative timing of their expression has not been accurately determined. Differences could also be due to deletion efficiency; we found that KDM5C deletion was more efficient in $Kdm5c^{\Delta Itgax}$ DCs compared with $Kdm5c^{\Delta Zbtb46}$ DCs (Figure S1D). In addition to differences in the timing of *Cre* transgene expression and deletion efficiency, the difference in the cDC2 populations in the $Kdm5c^{\Delta Zbtb46}$ and $Kdm5c^{\Delta Itgax}$ mice could be a result of environmental differences due to KDM5C deletion in other cell types, since *Itgax-Cre* expression is less restricted than *Zbtb46*-Cre. pDC expression of CRE is one of the primary differences between the *Itgax-Cre* and *Zbtb46-Cre*. Therefore, we examined the pDC populations in the $Kdm5c^{\Delta Itgax}$ mice. We found that a significant proportion of splenic pDCs (Lineage($B220^+CD3^+Ly6G^+CD19^+NK1.1^+$) $SiglecH^+CD11c^{int}$ $CD11b^-PDCA1^+$) in the $Kdm5c^{\Delta Itgax}$ mice did not express Ly6C (Figure 1B). This $Ly6C^-$ population was increased by more than 4-fold compared with the controls. The proportion of splenic $Ly6C^+$ pDCs was lower in $Kdm5c^{\Delta Itgax}$ due to the increase in $Ly6C^-$ pDCs, although the cell count was unchanged (Figure 1B).

To assess intrinsic versus extrinsic effects of KDM5C loss on DC heterogeneity, we generated mixed BM chimeric mice. We reconstituted the BM of CD45.1 mice (controls) with either an equal mix of $CD45.1^+$ control and $CD45.2^+$ $Kdm5c^{\Delta Itgax}$ BM (knockout), or of $CD45.2^+$ $Kdm5c^{\Delta Itgax}$ BM alone. We found the BM of each genotype reconstituted similar numbers of DCs; however, the differences in the cDC and pDC population compositions were similar to control and $Kdm5c^{\Delta Itgax}$ mice (Figures 1C and S1E). These data suggest intrinsic regulation of DC heterogeneity by KDM5C. To test whether pDCs themselves can affect cDC heterogeneity, pDCs in wild-type C57BL/6 mice were depleted by administering 250 μg anti-PDCA-1 antibody intraperitoneally every other day for 1 week *in vivo* (Figure S1F). Depletion of pDCs resulted in a small but significant increase in the proportion of cDC2B relative to cDC2A (Figure 1D), but without the changes in cDC1 and cDC2A population sizes seen in the $Kdm5c^{\Delta Itgax}$ mice (Figures 1D and S1G). Since one of the primary roles of pDCs is to produce type I IFN, we examined mice deficient in IFNAR1, the receptor for IFN-α and IFN-β, to test if type I IFN can shape the cDC population. Deficient IFN signaling led to moderate changes in proportions of cDC2 subsets comparable to pDC depletion, but did not affect cDC1s (Figures 1E and S1H). Collectively, these data suggest that the deletion of KDM5C intrinsically affects DC heterogeneity and that pDCs and type I IFNs can also shape the constitution of the cDC population.

KDM5C deficiency alters DC precursor populations

We next profiled BM cDC and pDC precursors using recent gating strategies[8,15,38] (Figure S2A) to determine if KDM5C loss affects DC precursor populations. No differences were found in total BM cell counts (Figure S2B) or myeloid-derived precursors ($Lin^{-}CD45^{+}CD11c^{-}MHCII^{-}FLT3^{+}cKIT^{hi}CD115^{+}$) (Figures S2A and S2C). We did, however, find decreased numbers of total common DC progenitors (CDPs; $Lin^{-}CD45^{+}CD11c^{-}MHCII^{-}FLT3^{+}cKIT^{mid}$) (Figures S2A and S2C). $CD115^{+}$ CDP (pre-cDC primed) populations were comparable with controls, whereas *Kdm5c*$^{\Delta Itgax}$ mice had decreased numbers of pre-pDC primed $CD115^{-}$ CDP populations[15,39] (Figure S2C). However, pre-pDCs described as $CD115^{-}CD127^{+}SiglecH^{+}Ly6D^{+}$[8] were unaffected by loss of KDM5C (Figure S2D). We also examined the pDC precursor pro-pDC described as $CD115^{-}SiglecH^{+}CD127^{+/-}$ $Ly6D^{+}$[16], and found they were decreased in *Kdm5c*$^{\Delta Itgax}$ mice (Figure S2E). Together, these findings show that, overall, pDC precursors are reduced in the absence of KDM5C.

We next examined pre-DCs ($Lin^{-}MHCII^{-}CD11c^{+}FLT3^{+}CD172^{-}$) in the BM that are delineated by Ly6C and SiglecH expression[15] (Figures 2A and S2A). We found increased proportions of both $Ly6C^{+}SiglecH^{+}$ pre-DCs (cDC2 primed) and $Ly6C^{-}SiglecH^{+}$ (pDC and cDC primed) in the *Kdm5c*$^{\Delta Itgax}$ mice and a decrease in $Ly6C^{+}$ $SiglecH^{-}$ pre-cDC2 proportions (Figure 2A). No differences were observed in the committed pre-cDC1s ($Ly6C^{-}SiglecH^{-}$) populations. The decrease in precDC2s may explain the decrease in cDC2A in *Kdm5c*$^{\Delta Itgax}$ mice.

Splenic populations termed transitional DCs (tDCs) and pDC-like cells have been identified to have characteristics of pDCs and can transition to cDC2 populations.[7,14,38,40,41] We examined these populations from control and *Kdm5c*$^{\Delta Itgax}$ mice using established gating strategies[7,14,38,40,41] (Figure S2F). While no differences were found in the proportions of $tDC^{hi/lo}$, we found an increase in tDC^{hi} cell counts (Figure 2B). Similar patterns were observed for pDC-like cells defined as $Lin^{-}MHCII^{-}CD11c^{hi}$ $SiglecH^{+}CX3CR1^{+}$ (Figure 2C). Consistent with previous reports,[38,40] pre-cDC1 overlap with the tDC population (Figure S2G). Importantly, these precursor populations are distinct from the $Ly6C^{-}$ pDCs, as $Ly6C^{-}$ pDCs express PDCA-1 and not CX3CR1 (Figure 2D). Together these results demonstrate that KDM5C expression affects the proportion of cDC and pDC precursors, however these precursor cells are distinct from the $Ly6C^{-}$ pDCs.

$Ly6C^{-}$ pDC are functionally distinct from $Ly6C^{+}$ pDCs

$Ly6C^{-}$ pDCs are a relatively undescribed population. To determine if $Ly6C^{-}$ and $Ly6C^{+}$ pDCs are functionally distinct, we first examined the expression of activation markers CD86, CD80, MHCII, PD-L1, and CD40. $Ly6C^{-}$ pDCs have a significantly lower expression of these surface markers compared with $Ly6C^{+}$ pDCs, suggesting they are less activated (Figure 3A). Transcriptional analyses revealed that $Ly6C^{-}$ pDCs have increased enrichment of genes associated with the cell cycle, whereas $Ly6C^{+}$ pDCs have increased enrichment of C-type lec-tins and IL-4 and IL-13 signaling (Figures 3B and S3A). pDCs are terminally differentiated and are known to have low proliferation potential[42]; therefore, these data suggest that the $Ly6C^{-}$ pDCs still have proliferative capacity and are less mature.

Ly6C$^-$ pDCs have similar expression of pDC markers, with the exception of reduced geometric mean fluorescence intensity of PDCA-1 and decreased proportion of CCR9$^+$ pDC in the BM (Figure 3C). CD4$^-$ pDCs have been shown to be a less mature subset of pDC[42]; we, therefore, examined whether Ly6C expression correlates with CD4 expression on pDCs. Ly6C$^-$ and CD4-expressing cells do not co-segregate; however, CD4$^-$ pDCs have a greater proportion of Ly6C$^-$ cells compared with CD4$^+$ pDCs (Figure 3D). Further, we found a greater frequency of Ly6C$^-$ pDCs in the BM, where pDC development takes place, compared with the spleen (Figure 3D). Collectively, these data suggest Ly6C$^-$ pDCs are less mature than Ly6C$^+$ pDCs.

To examine how the Ly6C$^-$ pDC populations change following immune activation, we examined pDC populations in uninfected controls and mice infected with lymphocytic choriomeningitis virus Armstrong (LCMV) for 20 h. We found that Ly6C$^-$ pDC numbers were decreased in the spleen after infection (Figure 3E). LCMV infection induces the production of type I IFNs, which promotes DC maturation. To test the effect of IFN-β on the Ly6C$^{+/-}$ pDC populations, BM precursors were differentiated to DCs with FLT3L *in vitro*. The generation of Ly6C$^+$ pDCs was enhanced by the addition of IFN-β (Figure S3B), suggesting that Ly6C$^-$ pDCs may become Ly6C$^+$ in the context of type I IFN. We used IFNAR1-deficient mice to determine if type I IFN affects the proportions of Ly6C$^-$ and Ly6C$^+$ pDC. *Ifnar1*$^{-/-}$ mice had more Ly6C$^-$ pDCs and fewer Ly6C$^+$ pDCs compared with controls (Figure 3F), suggesting that type I IFN may support the conversion of Ly6C$^-$ to Ly6C$^+$ pDCs. To test whether Ly6C$^-$ pDCs could become Ly6C$^+$ pDCs, we sorted Ly6C$^-$ pDCs by fluorescence-activated cell sorting (FACS) from control mice and stimulated them with the Toll-like receptor (TLR) ligand CpG ODN 1585. Approximately one-half of the Ly6C$^-$ pDCs became Ly6C$^+$ after TLR9 stimulation (Figure 3G). Collectively, these data suggest that Ly6C$^-$ pDCs are less mature compared with Ly6C$^+$ pDCs and that Ly6C$^-$ pDCs can convert to Ly6C$^+$ pDCs in inflammatory environments.

Mature pDCs are known for their superior ability to produce type I IFN, compared with less mature pDC, which in turn have greater ability to present antigen to T cells. We stimulated FACS-sorted Ly6C$^-$ and Ly6C$^+$ pDCs with CpG and found that indeed Ly6C$^-$ pDC produced less IFN compared with Ly6C$^+$ pDCs (Figure 3H). To test antigen presentation, we sorted Ly6C$^-$ and Ly6C$^+$ pDCs by FACS, and incubated with ovalbumin (OVA) protein and OTI CD8 T cells, which express T cell receptors (TCRs) specific for OVA. Both populations stimulated naive OTI CD8 T cells, and Ly6C$^-$ pDC had superior capacity to stimulate the proliferation of CD8 T cells compared with Ly6C$^+$ pDCs (Figure 3I). Together, these findings demonstrate that Ly6C$^-$ pDCs are a subset of pDCs that are poor producers of type I IFN, but are capable of presenting soluble antigens to CD8 T cells at steady state.

KDM5C promotes pDC function

Next, we examined the effect of KDM5C deletion on Ly6C$^-$ and Ly6C$^+$ pDC function. DCs from KDM5C-deficient animals had increased expression of the activation markers CD80, MHCII, and PD-L1 in both Ly6C$^+$ and Ly6C$^-$ pDCs, and increased expression of CD40 by Ly6C$^-$ pDCs, compared with controls, suggesting that KDM5C-deficient pDCs were more activated (Figure 4A). The increased expression of activation markers was preserved

in KDM5C-deficient cells in the mixed BM chimeras, suggesting intrinsic regulation (Figure 4B). Both splenic and BM KDM5C-deficient pDC populations had comparable expression of pDC lineage and maturation markers SiglecH, CX3CR1, and CCR9 compared with controls (Figures 4C and S4A).

KDM5C is a transcriptional regulator; therefore, we examined the transcriptomes of sorted control and KDM5C-deficient Ly6C^{-} and Ly6C^{+} pDCs (Figure S4B) from mice injected with PBS or LCMV (20 h) (Figures 4D, S4B, and S4C). KDM5C-deficient Ly6C^{-} and Ly6C^{+} had approximately 1,000 differentially expressed genes (DEGs) (false discovery rate of 0.05) compared with controls. DEGs were enriched in both positive and negative regulation of the immune system and IFN signaling (Figures 4D and S4C). For example, *Irf3*, *Ifi27*, and *Irf4* were increased in KDM5C-deficient pDC at steady state, whereas *Irf8*, *Ifnar1/2*, and *Tyk2* were expressed lower at homeostasis and were not induced to the same levels as in control pDC (Figure 4D). Many IFN responsive genes, including *Irf6*, *Irf2*, *Jak1*, *Oas2/3*, and *Socs1/3*, were increased to a greater extent following LCMV infection, despite the significant decrease in *Ifnar1/2* and *Ifna* gene expression (Figure 4D). *Irf7*, which drives IFN production, was unchanged. We also found no evidence of impaired expression of TLR signaling pathway (*Tlr7*, *Tlr9*, *Myd88* or *Unc93b1*) (Figure S4D). Reduced expression of IRF8 and increased expression of IRF4 was validated by intracellular stain and flow cytometry (Figure S4E).

We also found that DEGs between control and KDM5C-deficient pDCs were enriched in antigen processing and presentation pathways. KDM5C-deficient Ly6C^{+} pDCs had increased expression of genes involved in major histocompatibility complex (MHC) I antigen presentation (Figure 4E). To test their ability to present antigen to T cells, we sorted control and KDM5C-deficient Ly6C^{+} pDCs by FACS and co-cultured them with 100 μg whole OVA and naive CD4 OT-II T cells or CD8 OTI T cells labeled with violet proliferation dye (Figure 4F). While neither genotype efficiently stimulated the expansion of CD4 OT-II cells (Figure 4F), KDM5C-deficient Ly6C^{+} pDCs were significantly better at stimulating CD8 OTI T cells than control Ly6C^{+} pDCs (Figure 4G). We also tested the antigen presentation capacity of Ly6C^{-} pDCs and found that KDM5C-deficient Ly6C^{-} pDCs stimulated CD8 T cells to a lesser extent compared with controls (Figure 4H). These data show that KDM5C deficiency affects the ability of pDCs to stimulate CD8 T cells.

To test the capacity of Ly6C^{+} pDCs to present antigens *in vivo* (Figure 4I), we infected control and *Kdm5c*$^{\Delta Itgax}$ mice with LCMV-ARM and sorted Ly6C^{+} pDCs the next day. pDCs were cultured with P14 CD8 T cells, which express a TCR specific for LCMV antigen presented on MHCI. Indeed Ly6C^{+} pDCs deficient in KDM5C, but not controls, were able to stimulate P14 CD8 T cells in the absence of exogenous antigens (Figures 4I and S4F), demonstrating their ability to stimulate viral-specific CD8 T cells in the context of infection. The ability of pDCs to produce IFN and present antigens are generally opposed[43]; therefore, we measured IFN-α production after stimulation with CpG A/B, a TLR9 agonist. We found that KDM5C-deficient pDCs did indeed produce less IFN-α, consistent with their superior ability to present antigens (Figures 4J and S4G).

Similar to KDM5C-deficient pDCs, exhausted pDCs that have been described in chronic viral infection also have elevated activation markers but fail to produce type I IFN.[44,45] To determine if an exhausted pDC phenotype was associated with changes in *Kdm5c* expression, we sorted exhausted splenic pDC from mice infected with LCMV-CL13 (8 days post infection [dpi]), a clonal strain of LCMV that promotes chronic viral infection. *Kdm5c* expression was significantly decreased in exhausted pDCs compared with control pDCs (Figure 4K). Together, our data show that decreased KDM5C expression either through genetic deletion or during infection leads to an activated phenotype, but functionally results in an increased ability to stimulate CD8 T cells and decreased ability to produce type I IFN.

KDM5C restrains inflammatory gene expression in cDC1s

In Figure 1, we showed that KDM5C deficiency altered the heterogeneity of the cDC population. Therefore, we also examined changes in gene expression in KDM5C-deficient cDC1, cDC2A and cDC2B, and found that KDM5C deletion resulted in the greatest effects on cDC1 (~2,000 DEGs) compared with ~600 and ~800 DE genes in cDC2A and cDC2B, respectively (Figures S5A and S5B). We found that *Kdm5c* expression was higher in cDC1 compared with cDC2s (Figure S5C), which may explain the enhanced effect of KDM5C deletion on cDC1 gene expression. KDM5C-deficient cDC1s displayed enrichment of transcripts encoding proteins in inflammatory pathways, cytokine pathways, defense to viral infection, immune cell activation, and IRF-regulated pathways (Figures 5A, 5B, and 5D). These data are consistent with our previous work in BMDCs showing that KDM5C restrains cDC activation.[34] We performed TF binding site analysis using Hypergeometric Optimization of Motif EnRichment (HOMER) on genes with significantly increased expression levels in KDM5C-deficient cDC1s compared with controls and found predominant enrichment of IRF family TF motifs (Figure 5C). This agreed well with our RNA-seq data, which indicated that the dysregulation of several *Irf* genes in the absence of KDM5C (Figure 5D). Specifically, *Irf7*, *Irf1*, *Irf4*, and *Irf2bpl* were significantly up-regulated in KDM5C-deficient cDC1 compared with controls. IRF proteins are well known to participate in DC activation and activate inflammatory pathways and, therefore, are likely the key mediators of the increased gene expression observed in KDM5C-deficient cDC1.

KDM5C modifies chromatin structure by regulating the levels of H3K4me3, a histone post-translational modification associated with active chromatin state and gene transcription. We examined H3K4me3 levels by Cleavage Under Targets and Release Using Nuclease (CUT&RUN)[19,26] on approximately 20,000 sorted cells of each subset. We found 1,063 regions with increased levels of H3K4me3 in KDM5C-deficient cDC1s, compared with 22 regions with decreased H3K4me3, consistent with KDM5C being an H3K4 demethylase (Figure 5E). The majority of the differentially methylated regions were found in intronic and intergenic regions, suggesting that KDM5C loss affects enhancer elements and/or results in spurious transcription, as previously reported[29,46] (Figure S5E). To understand how changes in H3K4 trimethylation correspond with changes in gene expression in KDM5C-deficient DCs, we analyzed H3K4me3 levels in genes that were up- or down-regulated in our RNA-seq analysis (Figure 5E). As expected, we found regions with increased H3K4me3 annotated to genes that were up-regulated in KDM5C-deficient cDC1s (Figure 5E). Surprisingly, we also found increased H3K4me3 associated with genes that showed

no difference or decreased expression (Figure 5E). Because H3K4me3 in intergenic regions does not predictably change gene expression, we examined the change in expression of genes with differential levels of H3K4me3 in their promoters/gene bodies and found that, with a few exceptions, the majority of genes with increased H3K4me3 had increased gene expression in KDM5C-deficient cDC1 (Figure S5F). We performed pathway analyses on genes associated with regions with increased H3K4me3 and found enrichment of immune pathways associated with activation (Figure 5F).

Genes that were up-regulated, such as *Ifi27* and *Il10*, were commonly associated with increased H3K4me3 and H3K27ac (a marker of active chromatin, determined by CUT&RUN) (Figure 5G). *Cd207* was the only gene to show both down-regulation of gene expression and decreased H3K4me3 in the promoter region. Decreased expression of other genes such as *Itbp2* did not show corresponding changes in H3K4me3 or H3K27ac, suggesting alternative regulatory mechanisms are at play (Figure 5G). Together, these data support our model in which KDM5C restricts DC activation through the specific demethylation of pro-inflammatory genes, but can also promote gene expression through alternative mechanisms.

Overall, cDC1 from *Kdm5c*$^{\Delta Itgax}$ mice show an enhanced activation phenotype. To examine their ability to stimulate CD8 T cells, we sorted cDC1 from *Kdm5c*$^{\Delta Itgax}$ and control mice and incubated them with soluble OVA and OTI CD8 T cells. KDM5C-deficient cDC1 had a better ability to stimulate CD8 T cells compared with controls (Figures 5H and S5G). Together, these results show that KDM5C is an essential repressor of inflammatory gene expression and stimulatory capacity of cDC1 through regulating H3K4me3 levels.

KDM5C regulates OXPHOS gene expression and mitochondrial function in cDC1

As shown in Figure 5A, pathway enrichment analysis of our RNA-seq data identified the decreased abundance of transcripts associated with mitochondrial metabolism, including oxidative phosphorylation, in KDM5C-deficient cDC1s (Figure 6A). Since bioenergetic metabolism is important for the function of DCs,[47–50] we sought to determine if decreased expression of mitochondrial metabolism genes results in altered mitochondrial function. We first analyzed mitochondrial content and membrane potential using the mitochondrial dyes MitoSpy Green and TMRM, respectively. We found that, with KDM5C deficiency, mitochondrial mass was lower, as was mitochondrial membrane potential (Figure 6B). However, when graphed as a ratio, KDM5C-deficient cDC1 had increased membrane potential relative to mitochondrial mass, suggesting higher ETC activity per mitochondria. These differences were not due to changes in cell size (Figure S6A).

To assess how these changes in mitochondria resulted in differences in cellular bioenergetics, we used a Seahorse bio-analyzer to measure cellular respiration. We found that KDM5C-deficient cDC1s had a lower baseline oxygen consumption rate (OCR) compared with the control, in two of three experiments (three individual mice per group per experiment) (Figure 6C). Seahorse analysis uses the addition of several mitochondrial inhibitors to test the contribution of various mitochondrial processes to cellular OCR and provide insights into the causes of mitochondrial dysfunction. Oligomycin addition blocks the F_1F_0-ATPase and thus leftover OCR is due to proton leak into the mitochondrial matrix

and/or non-mitochondrial respiration. KDM5C-deficient cDC1s displayed a lower OCR after oligomycin treatment (coupled respiration) in two of three experiments, but also had lower levels of proton leak (Figures 6C and S6B). Reduced proton leak can cause an increase in proton buildup in the intermembrane space and likely explains the enhanced mitochondrial membrane potential per mass that we observed using TMRM and MitoSpy Green. Since proton leak occurs passively or actively through uncoupling proteins (UCPs), we examined gene expression of UCPs in cDC1, and found a decrease in the expression of UCP2 (adjusted p = 1.08E-06), potentially explaining the reduced levels of proton leak. Maximal respiratory capacity (MRC) is commonly assessed by measuring OCR after the addition of the mitochondrial uncoupler FCCP, which allows the release of protons from the inter-membrane space, and results in maximal oxygen consumption as the mitochondria attempt to replenish membrane potential. Reduced proton leak would result in increased MRC due to accumulation of protons in the intermembrane space. There was indeed a significant increase in MRC in the *Kdm5c*$^{\Delta Itgax}$ versus control cDC1s (Figure 6C). Together, these data support a model in which, in the absence of KDM5C, changes in gene expression of OXPHOS genes and UCP2 result in lower overall mitochondrial mass and baseline respiration, but increased mitochondrial membrane potential per mitochondria and elevated MRC. These data also suggest that mitochondrial oxygen consumption is tightly coupled to ATP production in KDM5C-deficient cDC1s.

We examined H3K4me3 levels of OXPHOS genes with reduced expression in KDM5C-deficient cDC1. Surprisingly, we found that decreased expression was not associated with decreased H3K4me3 or decreased H3K27ac, a marker of active gene expression (Figures 6D and 6E). We performed HOMER analyses on the same genes and found enrichment for YY1 motifs (Figure S6C). YY1 promotes the expression of mitochondrial respiration genes[51] through interaction with PGC-1α.[51] YY1 also regulates gene expression through long-distance DNA looping systems involving promoter-enhancer or enhancer-enhancer interactions.[52] Together, these data strongly suggest that KDM5C is a key regulator of mitochondrial gene expression and function in cDC1s but does so independent of H3K4me3 regulation.

KDM5C expression in DCs is required for lineage-specific gene expression and DC function during infection

In Figure 5D, we show that KDM5C deficiency results in altered gene expression of several IRF family members, including *Irf8* and *Irf4*, which encode lineage-specifying TFs required for the generation and function of cDC1 and cDC2, respectively. We examined the expression of several lineage markers in KDM5C-deficient cDC1s and found decreased expression of several cDC1-specific genes including *Irf8*, *Xcr1*, *Batf3*, *Cadm1*, and an increase in cDC2-specific genes including *Ltb*, *Cd4*, *Irf4*, *Itgam*, and *Tbx21*. Further, expression of *Tbx21*, which encodes cDC2A-specific TF T-BET recently shown to demarcate cDC2As, was reduced in cDC2As to levels found in cDC2Bs (Figure 7A). Like the mitochondrial genes, changes in gene expression were not strongly associated with changes in H3K4me3 at promoters (Figure 7B). We confirmed decreased IRF8 expression by flow cytometry (Figure 7C); however, even though *Irf4* expression was significantly different between control and KDM5C-deficient cDC1 (adjusted p =

4.59527E-13) IRF4 protein levels were not significantly reduced (Figure 7C). IRF8 expression is needed for cDC1 generation yet *Kdm5c*$^{\Delta Itgax}$ mice showed relatively normal cDC1 generation. Therefore, we examined IRF8 expression in pre-cDC and, consistent with other studies,[24,53,54] found that IRF8 is expressed in all pre-DCs and IRF8 expression was not affected by KDM5C loss (Figure S7A). This likely explains why cDC1 differentiation is not defective in the absence of KDM5C. Thus, the lineage-specific transcriptional programs that are important for DC identity, differentiation, and function are in part regulated by KDM5C.

Because DCs are not required for T cell priming during LCMV infection,[55] we used the *Listeria monocytogenes* infection model, in which proper cDC1 abundance and function are crucial for activating CD8 T cells,[56] to test whether the function of DCs is altered in the absence of KDM5C. Control and *Kdm5c*$^{\Delta Itgax}$ mice were infected with *L. monocytogenes* expressing OVA (*Lm*-OVA). At 1 dpi, serum was collected to measure IFN-α, and cDC1s were sorted to perform antigen presentation assays (Figure 7D). *Kdm5c*$^{\Delta Itgax}$ mice had reduced serum IFN-α, compared with controls (Figure 7E). To measure antigen presentation capacity, sorted cDC1s were cultured directly with OVA-specific OTI CD8 T cells without the addition of exogenous antigen. *Kdm5c*$^{\Delta Itgax}$ cDC1 had a decreased capacity to stimulate OTI T cells directly *ex vivo*, demonstrating a lower ability to present bacterial antigens after infection (Figure 7F). At 7 dpi, altered proportions of cDC and pDC subsets remained similar to those at homeostasis, with *Kdm5c*$^{\Delta Itgax}$ mice exhibiting increased proportions of cDC1, cDC2B, and Ly6C^{-} pDCs and decreased proportions of cDC2A and Ly6C^{+} pDCs in (Figures S7B and S7C). *Kdm5c*$^{\Delta Itgax}$ mice were also deficient in stimulating *Lm*-OVA-specific CD8 T cells *in vivo*. The proportion and number of OVA-specific CD8 T cells (tetramer^{+}) was reduced in *Kdm5c*$^{\Delta Itgax}$ mice (Figures 7G and S7D). As well, *Kdm5c*$^{\Delta Itgax}$ CD8 T cells were less functional, as measured by decreased IFN-γ^{+} and IFN-γ^{+} tumor necrosis factor - (TNF-α)$^{+}$ polyfunctional CD8 T cell populations (Figures 7H and S7E). There were no significant differences between control and *Kdm5c*$^{\Delta Itgax}$ mice in CD11a^{+}CD49d^{+} antigen-experienced or CD44^{+} effector CD4 T cells (Figures 7I and S7F). Thus, KDM5C expression in cDC1s is necessary to stimulate proper CD8 T cells responses during infection.

DISCUSSION

Immune protection requires that immune responses be tailored to the infection or insult. DCs are among the first responders, and as a whole are specialized in antigen presentation and cytokine production. However, several subsets exist within the DC population whose functions are further specialized. Significant advances of the mechanisms that guide DC specification into these subsets are continuously being made.[7–9,14,16,18] While several TFs have been demonstrated to be important for DC specification,[1,2,17,18] our results show that histone-modifying enzymes such as KDM5C also influence DC fate. Our work implicates KDM5C as a key regulator of the composition of both pDC and cDC populations and their functions. In the absence of KDM5C, pDC and cDC population heterogeneity as well as their functions are altered. KDM5C is not, however, absolutely required to generate a specific subset. Rather, it alters the proportions of subsets through modifying the epigenome and gene expression. Our data show that KDM5C is also important for functional responses

of pDCs and cDCs, and that mice without KDM5C expression in DCs mount impaired CD8 T cell response to *Listeria* infection.

Here, we identified a population of pDCs that are Ly6C^{-} and are more prevalent in *Kdm5c*$^{\Delta Itgax}$ mice. Ly6C^{-} pDC are not well studied, although one study also shows they produce less type I IFN than Ly6C^{+} cells.[57] Several lines of evidence from our work suggest that Ly6C^{-} pDCs are an immature pDC population; they have increased expression of cell-cycle genes; their abundance is greater in the bone marrow, where pDC maturation occurs; they are more capable of antigen presentation to T cells; and infection, IFN-β, and TLR-9 agonists induce a significant proportion of Ly6C^{-} pDCs to become Ly6C^{+}. Evidence of pDC antigen presentation has been largely in the context of CD4 T cell activation. However, we found here that pDCs can also activate CD8 T cells in an antigen-specific manner in response to both extracellular and endogenous antigens, consistent with previous studies.[58,59] Further work investigating the contribution of pDC antigen presentation to CD8 T cells to overall host immunity is warranted. Previous studies showed that CD4^{+} pDC are less migratory and produce lower levels of cytokines in response to stimulation compared with CD4^{-} pDC.[42] However, in our data, Ly6C and CD4 expression did not co-segregate, suggesting they are not the same populations. This raises the possibility that there may be subsets within the Ly6C^{-} population that have distinct antigen presentation and cytokine production capabilities. Further analyses at the single cell level are needed to understand the relationship between these subsets and pDC functions.

Recent studies highlight the heterogeneity and diverse functions of pDC-like cells. Murine pDC-like (Lin^{-}PDCA1^{+}SiglecH^{+} ZBTB46^{+}) cells and tDCs (Lin^{-}CD11b^{low}CD11c^{+}SiglecH^{+} CX3CR1^{+}PDCA1^{+}) resemble pDCs, but share some characteristics and transcriptional similarities to cDCs.[7,14] The pDC-like population has been described to serve as a progenitor pool for cDC2s.[7] The specialized tDC exhibits an enhanced capacity for antigen presentation compared with pDCs and a limited ability to produce type I IFNs, and can be further divided into CD11c^{low} tDC (Ly6C^{+}) and CD11c^{high} tDC (Ly6C^{-}).[14] Although the Ly6C^{-} pDCs that were enriched in *Kdm5c*$^{\Delta Itgax}$ mice in our study had impaired type I IFN production, they were not equivalent to the pDC-like or tDCs described in these other studies because they are B220^{+}, CCR9^{+}, and CX3CR1^{-}.

KDM5C-deficient Ly6C^{+} pDCs have an activated phenotype but are functionally impaired, which is a phenotype similar to that of exhausted pDCs.[44,45] Interestingly, we found that *Kdm5c* expression is decreased in exhausted pDCs from chronically infected mice. Our results suggest that the lower level of KDM5C expression in exhausted pDCs contributes to their dysfunction. KDM5C restrains the expression of immune response genes in pDCs, and the lack of this restraint likely contributes to their decreased ability to function as a high type I IFN-producing cell. KDM5C-deficient pDCs also have decreased IRF8 expression, which could contribute to the overall decreased ability to produce type I IFN. That said, we did not find differences in IRF8 expression between Ly6C^{-} and Ly6C^{+} pDCs.

We and others have found that, for some genes, KDM5C promotes their expression.[29,60,61] In this and our previous work,[61] loss of KDM5C leads to decreased gene expression of mitochondrial metabolism genes. The KDM5A-C *Drosophila* ortholog KDM5 (Lid)

also promotes the transcription of genes important for mitochondrial function.[60] However, KDM5 regulation of mitochondrial gene expression is mediated by the PHD3 domain, which is present in KDM5A/B but not KDM5C/D.[60] How KDM5C promotes transcription of these genes is not known. Positive regulation of gene expression by KDM5C has been linked to increased enhancer activity (by trimming H3K4me2/3 to H3K4me1) and co-activating gene expression.[29,46] We found an enrichment of YY1 binding motifs in promoters of mitochondrial metabolism genes reduced in KDM5C-deficient cDC1. YY1 is a TF that promotes mitochondrial gene expression, suggesting that KDM5C function may be linked to this pathway. Interestingly, YY1 regulates enhancer-enhancer, enhancer-promoter, and promoter-promoter loops,[52] suggesting that KDM5C may regulate gene expression through DNA loops. The implications of altered mitochondrial function for DC action are currently not clear; however, increased mitochondrial membrane potential to mass ratio has been associated with stress responses.[62] Our results also exemplify the importance of performing functional mitochondrial and metabolism assays to assess the consequences of changes in metabolic gene expression, which is often not linked to alterations in metabolic pathways.

We found a strong IRF signature in genes dysregulated by KDM5C deficiency in cDC1, which likely is responsible for the increased inflammatory gene expression at steady state. IRF8 and IRF4 are key TFs involved in DC specification of cDC1 and cDC2, respectively. Kim et al.[26] show that IRF4 and IRF8 do not specifically produce cDC2 and cDC1, but rather the amount of IRF protein determines their identity. While this study was focused on IRF4 and IRF8, it is not clear if other IRFs could also contribute to the tally of IRF that determine DC specificity. Deletion of IRF8 in committed cDC1s causes the cells to acquire a cDC2-like transcriptional signature and functional properties.[63] Despite decreased IRF8 in mature cDC1s from *Kdm5c*$^{\Delta Itgax}$ mice, cDC1 differentiate as normal. This is likely due to normal IRF8 expression in the pre-DCs. While KDM5C may directly regulate *Irf8* expression, we also found a decrease in *Batf3* expression, which is known to sustain *Irf8* expression in cDC1.[22] KDM5C regulates the balance of IRF4 and IRF8 expression in pDC and cDC, likely contributing to the changes in heterogeneity and function that we observe. However, we also find that KDM5C fine-tunes lineage-specific gene expression beyond IRF4 and IRF8. KDM5C-deficient cDC1 have increased expression of several cDC2-specific genes and a concomitant decreased expression of cDC1-specific genes. How KDM5C fine-tunes lineage-specific gene expression in DCs remains to be determined.

Epigenetic regulation of DC differentiation and function is well established.[64–66] Differentiation is generally accompanied by chromatin reprogramming that secures the differential gene expression necessary to establish cell type or cell states. KDM5C is a known H3K4me3 demethylase and, therefore, contributes to this chromatin remodeling. However, emerging studies point to demethylase-independent regulation of gene expression. In our studies, positive regulation of gene expression seems to be independent of H3K4me3 and, therefore, may be regulated by these alternative functions of KDM5C. Histone deacetylases have been shown to regulate gene expression necessary for DC differentiation and function.[67,68] Interestingly, three-dimensional enhancer networks controlled by CTCF, a well-known factor involved in forming topologically associated domains and chromatin loops, similar to YY1 mentioned above, also regulate epigenetic programming in DCs.[69]

Thus, chromatin structure modifiers are emerging as key regulators of DC specification and function.

The significance of cDC subset heterogeneity and how changes in heterogeneity alter inflammation and immunity is unclear. Because different subsets have specialized functions, it is likely that the composition of the DC population impacts the efficacy and efficiency of immune responses. The balance of DC subsets varies among mouse strains, individuals, lifespan, and during inflammation.[9,70–73] Our findings demonstrate that there are factors such as KDM5C that influence the balance of DC sub-types, along with the ability of the DC population as a whole to respond to infection. How KDM5C impacts DC specification and whether its expression or function is regulated during infection, aging, or across strains warrants further examination. Additional investigation into how the balance of subsets within the DC population affects immune responses will also provide further insight into how these cell types interact and work together to orchestrate a fully competent and efficient immune response in real world infection settings.

Limitations of the study

Our -omics analyses were performed on bulk populations of individual subsets. It is likely that there are subpopulations within these subsets, and differences in these subsets could account for the changes in gene expression and H3K4me3 levels. The same is true for flow gating strategies. Because we did not transfer control BM to $Kdm5c^{\Delta Itgax}$ mice we cannot conclude that the microenvironment in the $Kdm5c^{\Delta Itgax}$ mice has no effect on DC differentiation and function. Likewise, we did not analyze the DC precursors and pDC-like cells in these contexts. While we show many gene expression changes induced by KDM5C-loss, direct or indirect regulation cannot be inferred from our study.

STAR★METHODS

RESOURCE AVAILABILITY

Lead contact—Further information and requests for resources and reagents should be directed to and will be fulfilled by the lead contact, Connie Krawczyk (connie.krawczyk@vai.org).

Materials availability—Mouse lines generated in this study will be made available upon request with additional approval from Dr. Yang Shi. An agreement with our institute's Material Transfer Agreement may be required. No new reagents were created during this work.

Data and code availability—The bulk RNA-seq and CUT&RUN data have been deposited in the GEO repository under the GEO accession numbers GEO: GSE262866 and GEO: GSE263076. All packages for data processing in this study are listed in Method Details. This paper does not report original code. Any additional information required to reanalyze data reported in this text is available from the lead contact.

EXPERIMENTAL MODEL AND STUDY PARTICIPANT DETAILS

Mice—The following mouse strains were purchased from Jackson Laboratory and used for experiments and generating mouse lines used in this study; C57BL/6J (000664), *Ifnar*$^{-/-}$ (032045), *Zbtb*-Cre (028538), *Itgax*-Cre (008068), and Ly5.1 (002014). *Kdm5c*-fl/fl mice were a gift from the laboratory of Dr. Y. Shi.[29,61,86] *Kdm5c*-fl/fl mice were crossed to *Itgax* and *Zbtb* Cre strains to produce the conditional knockout animals used in this work. Control mice were *Kdm5cfl/fl*-Cre negative. All mice were bred and maintained in grouped housing at Van Andel Research Institute Vivarium under specific pathogen-free conditions. All procedures involving mice were completed as recommended in the Guide for the Care and Use of Laboratory Animals, and all protocols were approved by the IACUC committee of Van Andel Research Institute. Female mice were used for this study between the ages of 8–14 weeks. For each experiment,mice used were age matched.

The *Kdm5c* floxed strain was genotyped by PCR using the following primers:

Forward: 5′-CCATGGAGGCCAGAGAATAAG-3’

Reverse: 5′-CTCAGCGGATAAGAGAATTTGCTAC-3’

With the following PCR conditions 94°C-3m, 35x(94°C −30s, 58°C −30s, 72°C −30s), 70°C −2m, 4°C -end. The wild-type band is 120 bp and the mutant band is 170bp.

The *Itgax* Cre, *Zbtb* Cre mouse lines were genotyped by PCR using the following primers:

Cre Forward: 5′-AGATGCCAGGACATCAGGAACCTG-3’

Cre Reverse: 5′-ATCAGCCACACCAGACACAGAGATC-3’

Internal control Forward: 5′-CTAGGCCACAGAATTGAAAGATCT-3’

Internal control Reverse: 5′-GTAGGTGGAAATTCTAGCATCATCC-3’

With the following PCR conditions 94°C −2m, 10x(94°C −20s, 65°C −15s(−.5°C per cycle), 68°C −10s) 28x(94°C −15s, 60°C −15s, 72°C −10s), 72°C −2m, 4°C -end. The internal control band is 324bp and the mutant band is 236bp.

The *Ifnar*$^{-/-}$ strain was genotyped by PCR using the following primers:

Common Forward: 5′-CGAGGCGAAGTGGTTAAAAG-3’

Wild-type Reverse: 5′-ACGGATCAACCTCATTCCAC-3’

Mutant Reverse: 5′-AATTCGCCAATGACAAGACG-3’

With the following PCR conditions 94°C-3m, 35x(94°C −30s, 58°C −30s, 72°C −30s), 70°C −2m, 4°C -end. The wild-type band is 155bp and the mutant band is 250bp.

METHOD DETAILS

Tissue processing—Spleens were injected with HBSS (with Ca^{2+} and Mg^{2+}) containing 1 mg/mL of collagenase D and 10 μg/mL of DNase I (Roche) and incubated for 15 min at 37°C, followed by mashing and an additional 15 min incubation at 37°C. The cell suspension was passed through a 70 μm cell strainer, then spun down at 300 × g for 5 min. The cell pellet was resuspended in 1 mL of RBC lysis buffer (155 mM NH_4Cl, 12mM $NaHCO_3$, and 0.125 mM EDTA) for 2 min, followed by addition of 4 mL of complete medium. The cells are spun down at 300 × g for 5 min and resuspended at the desired volume and buffer for downstream use.

Mouse models

pDC depletion: Mice were injected intraperitoneally with 250 μg of α-PDCA-1 or IgG2b antibody (Bio Xcell) in 100 μL of PBS every other day. Five days following the first injection, pDC depletion was confirmed in blood collected by retro-orbital bleed and stained for flow cytometry analysis. Following confirmation of pDC depletion, mice were sacrificed the next day and spleens were removed and processed to analyze by flow cytometry.

Bone marrow chimera—Ly5.1 mice were irradiated with two doses of 450 rad 4 h apart. The next day, bone marrow from age-matched Ly5.1 mice (Control) and *Kdm5c*$^{\Delta Itgax}$ mice were extracted from the femurs and tibia. Cells were counted and resuspended to 25 × 10^6 non-RBCs per mL of PBS. 200 μL (5 × 10^6) of bone marrow cells from Ly5.1, *Kdm5c*$^{\Delta Itgax}$, or a 1:1 mix of Ly5.1 and *Kdm5c*$^{\Delta Itgax}$ were intravenously injected per irradiated Ly5.1 mouse. Mice were kept on drinking water containing 0.17 mg/mL of enrofloxacin (pH 3.0) for 2 weeks. Spleen and bone marrow were collected and processed 7 weeks post-injection to examine by flow cytometry.

LCMV infection—Mice were infected with 2 × 10^5 PFU of LCMV Armstrong, which was diluted in PBS from a frozen stock and delivered intraperitoneally in a BSL2 biosafety cabinet. Infected mice were housed in a separate quarantine room and monitored for the indicated length of time until tissues were collected and processed.

Listeria infection—Attenuated *Listeria monocytogenes* expressing ovalbumin (*Lm*-OVA) was grown in Tryptic Soy Broth containing streptomycin for 2–3 h at 37°C and 250 rpm. Once an OD600 of 0.6–0.8 was reached, the bacteria were pelleted and diluted in PBS to a concentration of 2 × 10^7 CFU/mL. Listeria was administered intravenously at 2 × 10^6 CFU per mouse in a BSL2 biosafety cabinet. Mice were housed in a separate quarantine room and monitored for 7 days until tissues were harvested for immunophenotyping. For *ex vivo* analyses, splenocytes from mice infected for 7 days with *Lm*-OVA were harvested and plated at 2×10^6/well in a 96-well non-tissue culture-treated plate. Cells were washed and stimulated in the presence of $OVA^{257–264}$ (1 μg/mL) (Anaspec), recombinant murine IL-2 200 U/ml (Peprotech) and 1x Brefeldin A (BioLegend) at a final volume of 200 μL for 5.5 h at 37° C in a humidified incubator. Following stimulation, cells were washed and processed for flow cytometry.

Flow cytometry—Samples were incubated with Fc block and eFluor 506 Fixable Viability Dye (ThermoFisher) in PBS, followed by an antibody cocktail prepared in wash buffer (PBS with 1% FBS, 1 mM EDTA, and 0.05% NaN_3). For intracellular staining, cells were fixed with IC fixation buffer (eBioscience/ThermoFisher) for 30 min following surface staining, permeabilized using Permeabilization Buffer (eBioscience/ThermoFisher) and incubated for at least 1 h with antibodies targeting intracellular proteins. Samples were acquired on the Cytek Aurora spectral cytometer and data analyzed using FlowJo v10. For mitochondrial staining, cells were plated and warmed to 37°C before staining. Mitochondrial dyes MitoSpy Green (BioLegend, 424806) and TMRM (ThermoFisher Scientific, T668) were prepared at 2x in HBSS, warmed, and added 1:1 to plated cells. Plates were incubated at 37°C for 20 min, washed, and surfaced stained. Cell sorting was performed on a Symphony S6 (BD Biosciences) or Moflo Astrios EQ Sorter (Beckman Coulter).

Antigen presentation—FACS-sorted splenic pDCs or cDC1s from *Kdm5c*$^{\Delta Itgax}$ and control mice at steady state infected with either LCMV or *Lm*-OVA for 1 day. DC subsets were combined based on genotype. The maximum number of replicates (min 3) were plated and based on the number of cells collected. At minimum 15,000 pDCs or 25,000 cDC1 were plated per replicate. pDCs were plated with either naive P14 for LCMV-ARM infection or OTI for *Lm*-OVA infection with or without 100μg OVA (Worthington). Naive CD8 T cells were labeled with VPD at a 1:3 ratio and cultured for 3 days. Flow analysis was done to assess proliferation. Cell counts were determined by gating live, $CD8^+CD44^+$, VPD diluted.

IFN-α enzyme-linked immunosorbent assay (ELISA): $Ly6C^+$ and $Ly6C^-$ pDCs that are $PDCA\text{-}1^+B220^+CD11b^-$ $CD11c^{int}$ were sorted from *Kdm5c*$^{\Delta Itgax}$ or control spleens and samples were pooled together for biological replicates of 15,000 cells per well. Cells were resuspended in 100 μL of complete medium (RPMI 1640 and 10% FBS, 2 mM L-glutamine, 100 U/mL penicillin/streptomycin, 0.01% β-mercaptoethanol) prior to plating, and 2X treatment was added to each well in 100 μL of complete medium. Cells were treated with CpG ODN 1585 to stimulate IFN responses (Invivogen; catalog # tlr-kit9m). After treatment for 18 h, supernatant was collected and IFN-α measured by ELISA according to manufacturer's instructions (Invitrogen; catalog # BMS6027). Serum IFN-α ELISA: 1 dpi *Lm*-OVA serum was analyzed using BioLegend IFN-α ELISA kit performed in triplicate.

***In vitro* DC differentiation with FLT3L—**Mouse tibia and femur were washed with 70% EtOH followed by PBS, and bone marrow was extracted. 2×10^5 bone marrow cells (not counting RBC) were seeded per well in a 96-well plate in RPMI-1640 containing 10% FBS (NuSerum), 2 mM L-glutamine, 100 U/mL of penicillin/streptomycin, 0.55 μM β-mercaptoethanol, and 100 ng/mL FLT3L (Peprotech), with or without 50 U/mL IFN-β (PBL Interferon Source). After 3 days, 2.5×10^5 mitomycin-treated OP9-DL1 cells (kindly gifted by Boris Reizis laboratory) were seeded in a tissue culture-treated 96-well plate.[87] The OP9-DL1 cells were allowed to settle for approximately 2 h prior to transferring over the bone marrow cells with replenished media with 100 ng/mL FLT3L with or without IFN-β as before. After 4 additional days, cells were stained to analyze by flow cytometry.

Western blot—Protein lysates from FACS-sorted cDCs from control and *Kdm5c*$^{\Delta Itgax}$ or *Kdm5c*$^{\Delta Zbtb46}$ spleens were prepared using CHAPS lysis buffer (Cell Signaling, 9852S) with protease inhibitors (Roche, 11836170001), quantified with Pierce 660 nm Protein Assay Reagent (ThermoFisher Scientific; 1861426), and mixed with Laemmli sample buffer (BioWorld 10570021). 25 μg of protein per sample was loaded into 4–20% pre-cast polyacrylamide gels (Bio-Rad) and proteins were transferred to methanol-activated polyvinylidene fluo-ride membranes. Membranes were blocked for 1 h using 5% milk in Tris-buffer saline (TBS) containing 0.1% Tween 20 (TBS-T), followed by overnight incubation at 4°C with anti-KDM5C antibody (1:1000; Abcam; Ab194288) in 5% milk in TBS-T, or 1 h at room temperature with anti-β-actin antibody (1:1000; Cell Signaling; 4967S) in 5% bovine serum albumin (BSA) in TBS-T. Following washes with TBS-T, membranes were incubated with anti-rabbit horseradish peroxidase-linked antibody (Cell Signaling; 7074S) at a dilution of 1:4000 in 5% milk for 2 h at room temperature for KDM5C, or 1:10 000 in 5% milk for 1 h at room temperature for β-actin. Blots were developed by enhanced chemiluminescence using SuperSignal West Dura Extended Duration Substrate (ThermoFisher Scientific; 34075) and Bio-Rad ChemiDoc MP Imaging System.

Metabolic assay—Several metabolic parameters were assessed in sorted cDC1 using the XF Cell Mito Stress Test and Seahorse XFe96 Analyzer (Agilent). cDC1s were labeled with PE-XCR1 antibody for positive selection using magnet after pan-DC enrichment (Miltenyi). The cell plate was coated with poly-D-lysine, then 200,000 cells were seeded per well in XF RPMI medium containing 10 mM glucose and 2 mM L-glutamine, with pH adjusted to 7.4. The plate was then incubated at 37°C in a non-CO2 incubator for 1 h prior to the assay. Cells were sequentially treated with oligomycin (1.5 μM), FCCP (3 μM), and rotenone/antimycin A (0.5 μM), and oxygen consumption rate (OCR) was measured. At the end of each assay, cells were stained with Hoescht stain (20 μM; ThermoFisher Scientific) for 15 min at 37°C, then imaged using a Cytation imaging reader (Cytek) to count cells. OCR measurements were normalized by cell number.

RNA-seq—15,000 cells were FACS sorted into 1.5 mL tubes containing 350 μl lysis buffer. (Norgen Biotek buffer RL) RNA was extracted using Single Cell RNA Purification kit from Norgen Biotek (cat# 51800) and quantified using qubit HS RNA Assay kit (cat# Q32852). RNA libraries were generated using Takara SMARTer Stranded total RNA-seq Kit v3 (cat# 634487) and sequenced 50 bp, paired-end on an Illumina NovaSeq6000 sequencer. Reads were aligned to the mm10 genome and ERCC sequences using Takara's CogentAP v1.5, specifying the 'Strnd_UMI' kit configuration. The deduplicated (via UMIs) counts were imported into R v4.1.0 for further analysis. Genes with >2 counts in at least 2 samples were retained. Differential expression for pairwise contrasts was tested using DESeq2 v1.32.0[74] with a significance cutoff of 0.1 FDR; a model design of '~ Group' was used, where Group represents unique combinations of genotype, treatment and cell type. Log fold changes were shrunken using the 'lfcShrink' function, with the parameter, "type = 'ashr"'[88] and used to rank genes for GSEA analysis using clusterProfiler v4.0.5[75]).

CUT&RUN—Libraries for CUT&RUN-seq were prepared from 25,000 sorted cells.[89] Transposition and amplification reactions were performed using the Nextera DNA Library preparation kit (Illumina) and sequenced 50 bp, paired-end on an Illumina NovaSeq6000 sequencer. Reads were trimmed using TrimGalore v0.6.0 with default parameters and aligned to the mm10 genome and decoy sequences, including viral sequences and cfMeDIP-seq spike-in sequences[90,91] using bwa mem v0.7.17.[76] PCR duplicates were marked using SAMBLASTER v0.1.24.[77] Only high-confidence and properly-paired alignments were retained using samtools view with parameters, "-q 30 -f 2 -F 2828" (v1.9).[78] For peak calling, duplicate alignments were removed and processed with MACS2 v2.2.7.1[79] with the parameters, "-f BAMPE -g mm –keep-dup 'all"'. Called peaks were filtered to remove ENCODE blacklist v2 regions.[80] Bigwig files for visualization was produced using DeepTools v3.4.3[81]; bamCoverage was run with the parameters, "–binSize 10 –extendReads –normalizeUsing 'CPM' –samFlagExclude 1024 –samFlagInclude 64". Bigwig files were combined across replicates by finding the mean using WiggleTools v1.2.11[82] and wigToBigWig from UCSC tools. Coverage heatmaps were generated using Deeptools v3.4.3.

Differential PTM was tested using DiffBind v3.2.7.[83] For read counting, 'dba.count' was run with the parameters, 'summits = 200, bUseSummarizeOverlaps = TRUE', with SummarizeOverlaps configured to paired-end mode. For sample normalization, 'dba.normalize' was run with the parameters, 'normalize = DBA_NORM_NATIVE, background = TRUE'. The 'dba.analyze' step was run with the parameters, 'bBlacklist = FALSE, bGreylist = FALSE'. Pairwise contrasts between different combinations of genotype and cell type were tested using an FDR cutoff of 0.1. Significant peaks were annotated to their nearest gene using ChIPSeeker v1.28.3,[84] considering 3000 to +500 as the promoter region. For pathway enrichment analysis, peaks labeled as "Distal Intergenic" were removed and peaks were separated into up and down-regulated. Overlapping genes were tested using hypergeometric tests as implemented in clusterProfiler v4.0.5.

Heatmaps—Heatmaps were generated using pheatmap version 1.0.12 package in R (version 4.4.2).

HOMER analysis—The findMotifs.pl script in HOMER[85] version 4.11 was utilized to identify transcription factor binding sites (TFBS) using gene lists obtained from transcriptomics differential expression analyses. The search criteria for TFBS included lengths ranging from 8 to 10 bases, and their locations were restricted to within 2000 bases upstream and 100 bases downstream of the transcription start site (TSS).

QUANTIFICATION AND STATISTICAL ANALYSIS

Statistical analyses were performed using GraphPad Prism 10 software (Dotmatrics). When comparing two groups an unpaired two-tailed Welch's corrected t test were used to determine significance. When comparing means of more than 2 groups a one-ANOVA or unpaired multiple *t* test was used. A *p* value <0.05 was considered significant: $*p < 0.05$, $**p < 0.01$, $***p < 0.001$, $****p < 0.0001$. *p* values greater than 0.05 were considered nonsignificant (ns). The number of mice in each group and the number of replicates for

experiments were listed in the figure legends. The experiments were not randomized and experimenters were not blinded to genotypes. For RNA-seq, differential expression for pairwise contrasts was tested using DESeq2 v1.32.0[74] with a significance cutoff of 0.1 FDR. For Cut and Run, pairwise contrasts between different combinations of genotype and cell type were tested using an FDR cutoff of 0.1.

Supplementary Material

Refer to Web version on PubMed Central for supplementary material.

ACKNOWLEDGMENTS

We thank the members of the Krawczyk lab, Jones lab, and Scott Rothbart for input and scientific discussion contributing to this work. We thank Art Arnold and Yang Shi for the *Kdm5c-floxed* mice. This research was supported in part by the Van Andel Institute Cores (Flow Cytometry [RRID:SCR_022685], Genomics [RRID:SCR_022913], Bioinformatics and Biostatistics [RRID:SCR_024762], and Vivarium [RRID:SCR_023211]). Special thanks to Rachael Sheridan and Madison Nichols in the flow cytometry core for excellent service and Robert Binder for insights into MHC1 antigen presentation.

This project has been supported by CIHR SABV Catalyst grant and NIAID R21AI153997 to C.K.

REFERENCES

1. Merad M, Sathe P, Helft J, Miller J, and Mortha A (2013). The dendritic cell lineage: ontogeny and function of dendritic cells and their subsets in the steady state and the inflamed setting. Annu. Rev. Immunol. 31, 563–604. [PubMed: 23516985]
2. Ginhoux F, Guilliams M, and Merad M (2022). Expanding dendritic cell nomenclature in the single-cell era. Nat. Rev. Immunol. 22, 67–68. [PubMed: 35027741]
3. Schlitzer A, Zhang W, Song M, and Ma X (2018). Recent advances in understanding dendritic cell development, classification, and phenotype. F1000Res. 7, F1000 Faculty Rev-1558. 10.12688/f1000research.14793.1.
4. Brown CC, Gudjonson H, Pritykin Y, Deep D, Lavallée V-P, Mendoza A, Fromme R, Mazutis L, Ariyan C, Leslie C, et al. (2019). Transcriptional Basis of Mouse and Human Dendritic Cell Heterogeneity. Cell 179, 846–863.e24. [PubMed: 31668803]
5. Naik SH, Sathe P, Park H-Y, Metcalf D, Proietto AI, Dakic A, Carotta S, O'Keeffe M, Bahlo M, Papenfuss A, et al. (2007). Development of plasmacytoid and conventional dendritic cell subtypes from single precursor cells derived in vitro and in vivo. Nat. Immunol. 8, 1217–1226. [PubMed: 17922015]
6. Schlitzer A, Sivakamasundari V, Chen J, Sumatoh HRB, Schreuder J, Lum J, Malleret B, Zhang S, Larbi A, Zolezzi F, et al. (2015). Identification of cDC1- and cDC2-committed DC progenitors reveals early line-age priming at the common DC progenitor stage in the bone marrow. Nat. Immunol. 16, 718–728. [PubMed: 26054720]
7. Rodrigues PF, Kouklas A, Cvijetic G, Bouladoux N, Mitrovic M, Desai JV, Lima-Junior DS, Lionakis MS, Belkaid Y, Ivanek R, and Tussiwand R (2023). pDC-like cells are pre-DC2 and require KLF4 to control homeostatic CD4 T cells. Sci. Immunol 8, eadd4132. [PubMed: 36827419]
8. Rodrigues PF, Alberti-Servera L, Eremin A, Grajales-Reyes GE, Ivanek R, and Tussiwand R (2018). Distinct progenitor lineages contribute to the heterogeneity of plasmacytoid dendritic cells. Nat. Immunol. 19, 711–722. [PubMed: 29925996]
9. Guilliams M, Dutertre C-A, Scott CL, McGovern N, Sichien D, Chakarov S, Van Gassen S, Chen J, Poidinger M, De Prijck S, et al. (2016). Unsupervised High-Dimensional Analysis Aligns Dendritic Cells across Tissues and Species. Immunity 45, 669–684. [PubMed: 27637149]
10. Musumeci A, Lutz K, Winheim E, and Krug AB (2019). What Makes a pDC: Recent Advances in Understanding Plasmacytoid DC Development and Heterogeneity. Front. Immunol. 10, 1222. [PubMed: 31191558]

11. Villani A-C, Satija R, Reynolds G, Sarkizova S, Shekhar K, Fletcher J, Griesbeck M, Butler A, Zheng S, Lazo S, et al. (2017). Single-cell RNA-seq reveals new types of human blood dendritic cells, monocytes, and progenitors. Science 356, eaah4573. 10.1126/science.aah4573. [PubMed: 28428369]
12. Zhang H, Gregorio JD, Iwahori T, Zhang X, Choi O, Tolentino LL, Prestwood T, Carmi Y, and Engleman EG (2017). A distinct subset of plasmacytoid dendritic cells induces activation and differentiation of B and T lymphocytes. Proc. Natl. Acad. Sci. USA 114, 1988–1993. [PubMed: 28167780]
13. Alcántara-Hernández M, Leylek R, Wagar LE, Engleman EG, Keler T, Marinkovich MP, Davis MM, Nolan GP, and Idoyaga J (2017). High-Dimensional Phenotypic Mapping of Human Dendritic Cells Reveals Interindividual Variation and Tissue Specialization. Immunity 47, 1037–1050.e6. [PubMed: 29221729]
14. Leylek R, Alcántara-Hernández M, Lanzar Z, Lüdtke A, Perez OA, Reizis B, and Idoyaga J (2019). Integrated Cross-Species Analysis Identifies a Conserved Transitional Dendritic Cell Population. Cell Rep. 29, 3736–3750.e8. [PubMed: 31825848]
15. Dress RJ, Dutertre C-A, Giladi A, Schlitzer A, Low I, Shadan NB, Tay A, Lum J, Kairi MFB, Hwang YY, et al. (2019). Plasmacytoid dendritic cells develop from Ly6D+ lymphoid progenitors distinct from the myeloid lineage. Nature immunology 20, 852–864. 10.1038/s41590-019-0420-3. [PubMed: 31213723]
16. Feng J, Pucella JN, Jang G, Alcántara-Hernández M, Upadhaya S, Adams NM, Khodadadi-Jamayran A, Lau CM, Stoeckius M, Hao S, et al. (2022). Clonal lineage tracing reveals shared origin of conventional and plasmacytoid dendritic cells. Immunity 55, 405–422.e11. [PubMed: 35180378]
17. Anderson DA 3rd, Murphy KM, and Briseño CG (2018). Development, Diversity, and Function of Dendritic Cells in Mouse and Human. Cold Spring Harbor Perspect. Biol 10, a028613. 10.1101/cshperspect.a028613.
18. Murphy TL, Grajales-Reyes GE, Wu X, Tussiwand R, Briseño CG, Iwata A, Kretzer NM, Durai V, and Murphy KM (2016). Transcriptional control of dendritic cell development. Annu. Rev. Immunol. 34, 93–119. [PubMed: 26735697]
19. Nutt SL, and Chopin M (2020). Transcriptional Networks Driving Dendritic Cell Differentiation and Function. Immunity 52, 942–956. [PubMed: 32553180]
20. Satpathy AT, Briseño CG, Lee JS, Ng D, Manieri NA, Kc W, Wu X, Thomas SR, Lee W-L, Turkoz M, et al. (2013). Notch2-dependent classical dendritic cells orchestrate intestinal immunity to attaching-andeffacing bacterial pathogens. Nat. Immunol. 14, 937–948. [PubMed: 23913046]
21. Lukowski SW, Rødahl I, Kelly S, Yu M, Gotley J, Zhou C, Millard S, Andersen SB, Christ AN, Belz G, et al. (2021). Absence of Batf3 reveals a new dimension of cell state heterogeneity within conventional dendritic cells. iScience 24, 102402. [PubMed: 33997687]
22. Grajales-Reyes GE, Iwata A, Albring J, Wu X, Tussiwand R, Kc W, Kretzer NM, Briseño CG, Durai V, Bagadia P, et al. (2015). Batf3 maintains autoactivation of Irf8 for commitment of a CD8α(+) conventional DC clonogenic progenitor. Nat. Immunol. 16, 708–717. [PubMed: 26054719]
23. Bagadia P, Huang X, Liu T-T, Durai V, Grajales-Reyes GE, Nitschké M, Modrusan Z, Granja JM, Satpathy AT, Briseño CG, et al. (2019). An Nfil3-Zeb2-Id2 pathway imposes Irf8 enhancer switching during cDC1 development. Nat. Immunol. 20, 1174–1185. [PubMed: 31406377]
24. Sichien D, Scott CL, Martens L, Vanderkerken M, Van Gassen S, Plantinga M, Joeris T, De Prijck S, Vanhoutte L, Vanheerswynghels M, et al. (2016). IRF8 Transcription Factor Controls Survival and Function of Terminally Differentiated Conventional and Plasmacytoid Dendritic Cells, Respectively. Immunity 45, 626–640. [PubMed: 27637148]
25. Suzuki S, Honma K, Matsuyama T, Suzuki K, Toriyama K, Akitoyo I, Yamamoto K, Suematsu T, Nakamura M, Yui K, and Kumatori A (2004). Critical roles of interferon regulatory factor 4 in CD11bhighCD8alpha- dendritic cell development. Proc. Natl. Acad. Sci. USA 101, 8981–8986. [PubMed: 15184678]
26. Kim S, Bagadia P, Anderson DA, Murphy KM 3rd, Liu T-T, Huang X, Theisen DJ, O'Connor KW, Ohara RA, Iwata A, and Murphy TL (2021). High Amount of Transcription Factor IRF8 Engages

AP1-IRF Composite Elements in Enhancers to Direct Type 1 Conventional Dendritic Cell Identity. Immunity 54, 1622. [PubMed: 34260888]

27. Iwase S, Lan F, Bayliss P, de la Torre-Ubieta L, Huarte M, Qi HH, Whetstine JR, Bonni A, Roberts TM, and Shi Y (2007). The X-linked mental retardation gene SMCX/JARID1C defines a family of histone H3 lysine 4 demethylases. Cell 128, 1077–1088. [PubMed: 17320160]
28. Shen H-F, Zhang W-J, Huang Y, He Y-H, Hu G-S, Wang L, Peng B-L, Yi J, Li T-T, Rong R, et al. (2021). The Dual Function of KDM5C in Both Gene Transcriptional Activation and Repression Promotes Breast Cancer Cell Growth and Tumorigenesis. Adv. Sci 8, 2004635.
29. Outchkourov NS, Muiño JM, Kaufmann K, van Ijcken WFJ, Groot Koerkamp MJ, van Leenen D, de Graaf P, Holstege FCP, Grosveld FG, and Timmers HTM (2013). Balancing of histone H3K4 methylation states by the Kdm5c/SMCX histone demethylase modulates promoter and enhancer function. Cell Rep. 3, 1071–1079. [PubMed: 23545502]
30. Wu L, Cao J, Cai WL, Lang SM, Horton JR, Jansen DJ, Liu ZZ, Chen JF, Zhang M, Mott BT, et al. (2018). KDM5 histone demethylases repress immune response via suppression of STING. PLoS Biol. 16, e2006134. [PubMed: 30080846]
31. Chen K, Luan X, Liu Q, Wang J, Chang X, Snijders AM, Mao J-H, Secombe J, Dan Z, Chen J-H, et al. (2019). Drosophila Histone Demethylase KDM5 Regulates Social Behavior through Immune Control and Gut Microbiota Maintenance. Cell Host Microbe 25, 537–552.e8. [PubMed: 30902578]
32. Tricarico R, Nicolas E, Hall MJ, and Golemis EA (2020). X- and Y-Linked Chromatin-Modifying Genes as Regulators of Sex-Specific Cancer Incidence and Prognosis. Clin. Cancer Res. 26, 5567–5578. [PubMed: 32732223]
33. Doss PMIA, Umair M, Baillargeon J, Fazazi R, Fudge N, Akbar I, Yeola AP, Williams JB, Leclercq M, Joly-Beauparlant C, et al. (2021). Male sex chromosomal complement exacerbates the pathogenicity of Th17 cells in a chronic model of central nervous system autoimmunity. Cell Rep. 34, 108833. [PubMed: 33691111]
34. Boukhaled GM, Cordeiro B, Deblois G, Dimitrov V, Bailey SD, Holowka T, Domi A, Guak H, Chiu H-HC, Everts B, et al. (2016). The Transcriptional Repressor Polycomb Group Factor 6, PCGF6, Negatively Regulates Dendritic Cell Activation and Promotes Quiescence. Cell Rep. 16, 1829–1837. [PubMed: 27498878]
35. Audiger C, Fois A, Thomas AL, Janssen E, Pelletier M, and Lesage S (2020). Merocytic Dendritic Cells Compose a Conventional Dendritic Cell Subset with Low Metabolic Activity. J. Immunol. 205, 121–132. [PubMed: 32461238]
36. Lewis KL, Caton ML, Bogunovic M, Greter M, Grajkowska LT, Ng D, Klinakis A, Charo IF, Jung S, Gommerman JL, et al. (2011). Notch2 receptor signaling controls functional differentiation of dendritic cells in the spleen and intestine. Immunity 35, 780–791. [PubMed: 22018469]
37. Abram CL, Roberge GL, Hu Y, and Lowell CA (2014). Comparative analysis of the efficiency and specificity of myeloid-Cre deleting strains using ROSA-EYFP reporter mice. J. Immunol. Methods 408, 89–100. [PubMed: 24857755]
38. Valente M, Collinet N, Vu Manh T-P, Popoff D, Rahmani K, Naciri K, Bessou G, Rua R, Gil L, Mionnet C, et al. (2023). Novel mouse models based on intersectional genetics to identify and characterize plasmacytoid dendritic cells. Nat. Immunol. 24, 714–728. [PubMed: 36928414]
39. Tian Y, Guo X, Wu T, Fei K, and Wu L (2022). Identification of a novel cDC2-committed progenitor within mouse common dendritic cell progenitor population. Protein Cell 13, 302–307. [PubMed: 34981445]
40. Sulczewski FB, Maqueda-Alfaro RA, Alcántara-Hernández M, Perez OA, Saravanan S, Yun TJ, Seong D, Arroyo Hornero R, Raquer-McKay HM, Esteva E, et al. (2023). Transitional dendritic cells are distinct from conventional DC2 precursors and mediate proinflammatory antiviral responses. Nat. Immunol. 24, 1265–1280. [PubMed: 37414907]
41. Schlitzer A, Heiseke AF, Einwächter H, Reindl W, Schiemann, Manta C-P, See P, Niess J-H, Suter T, Ginhoux, and Krug AB (2012). Tissue-specific differentiation of a circulating CCR9- pDC-like common dendritic cell precursor. Blood 119, 6063–6071. [PubMed: 22547585]
42. Zhan Y, Chow KV, Soo P, Xu Z, Brady JL, Lawlor KE, Masters SL, O'keeffe M, Shortman K, Zhang J-G, and Lew AM (2016). Plasmacytoid dendritic cells are short-lived: reappraising the

influence of migration, genetic factors and activation on estimation of lifespan. Sci. Rep. 6, 25060. [PubMed: 27112985]

43. Reizis B (2019). Plasmacytoid Dendritic Cells: Development, Regulation, and Function. Immunity 50, 37–50. [PubMed: 30650380]
44. Macal M, Jo Y, Dallari S, Chang AY, Dai J, Swaminathan S, Wehrens EJ, Fitzgerald-Bocarsly P, and Zúñiga EI (2018). Self-Renewal and Toll-like Receptor Signaling Sustain Exhausted Plasmacytoid Dendritic Cells during Chronic Viral Infection. Immunity 48, 730–744.e5. [PubMed: 29669251]
45. Zuniga EI, Liou L-Y, Mack L, Mendoza M, and Oldstone MBA (2008). Persistent virus infection inhibits type I interferon production by plasmacytoid dendritic cells to facilitate opportunistic infections. Cell Host Microbe 4, 374–386. [PubMed: 18854241]
46. Scandaglia M, Lopez-Atalaya JP, Medrano-Fernandez A, Lopez-Cascales MT, Del Blanco B, Lipinski M, Benito E, Olivares R, Iwase S, Shi Y, and Barco A (2017). Loss of Kdm5c Causes Spurious Transcription and Prevents the Fine-Tuning of Activity-Regulated Enhancers in Neurons. Cell Rep. 21, 47–59. [PubMed: 28978483]
47. Krawczyk CM, Holowka T, Sun J, Blagih J, Amiel E, DeBerardinis RJ, Cross JR, Jung E, Thompson CB, Jones RG, and Pearce EJ (2010). Toll-like receptor-induced changes in glycolytic metabolism regulate dendritic cell activation. Blood 115, 4742–4749. [PubMed: 20351312]
48. Guak H, Al Habyan S, Ma EH, Aldossary H, Al-Masri M, Won SY, Ying T, Fixman ED, Jones RG, McCaffrey LM, et al. (2018). Glycolytic metabolism is essential for CCR7 oligomerization and dendritic cell migration. Nat. Commun. 9, 2463. 10.1038/s41467-018-04804-6. [PubMed: 29941886]
49. Guak H, Sheldon RD, Beddows I, Ark AV, Shen H, Jones RG, St-Pierre J, Ma EH, and Krawczyk CM (2022). PGC-1b maintains mitochondrial metabolism and restrains inflammatory gene expression. Sci. Rep. 12, 16028. 10.1101/2022.05.18.492477. [PubMed: 36163487]
50. Everts B, Amiel E, Huang SC-C, Smith AM, Chang C-H, Lam WY, Redmann V, Freitas TC, Blagih J, van der Windt GJW, et al. (2014). TLR-driven early glycolytic reprogramming via the kinases TBK1-IKKe supports the anabolic demands of dendritic cell activation. Nat. Immunol. 15, 323–332. [PubMed: 24562310]
51. Cunningham JT, Rodgers JT, Arlow DH, Vazquez F, Mootha VK, and Puigserver P (2007). mTOR controls mitochondrial oxidative function through a YY1-PGC-1alpha transcriptional complex. Nature 450, 736–740. [PubMed: 18046414]
52. Weintraub AS, Li CH, Zamudio AV, Sigova AA, Hannett NM, Day DS, Abraham BJ, Cohen MA, Nabet B, Buckley DL, et al. (2017). YY1 Is a Structural Regulator of Enhancer-Promoter Loops. Cell 171, 1573–1588.e28. [PubMed: 29224777]
53. Liu Z, Wang H, Li Z, Dress RJ, Zhu Y, Zhang S, De Feo D, Kong WT, Cai P, Shin A, et al. (2023). Dendritic cell type 3 arises from Ly6C+ monocyte-dendritic cell progenitors. Immunity 56, 1761–1777.e6. [PubMed: 37506694]
54. Kim S, Chen J, Jo S, Ou F, Ferris ST, Liu T-T, Ohara RA, Anderson DA, Wu R, Chen MY, et al. (2023). IL-6 selectively suppresses cDC1 specification via C/EBPb. J. Exp. Med. 220, e20221757. 10.1084/jem.20221757. [PubMed: 37432392]
55. Hilpert C, Sitte S, Matthies A, and Voehringer D (2016). Dendritic Cells Are Dispensable for T Cell Priming and Control of Acute Lymphocytic Choriomeningitis Virus Infection. J. Immunol. 197, 2780–2786. [PubMed: 27549169]
56. Edelson BT, Bradstreet TR, Hildner K, Carrero JA, Frederick KE, Kc W, Belizaire R, Aoshi T, Schreiber RD, Miller MJ, et al. (2011). CD8α(+) dendritic cells are an obligate cellular entry point for productive infection by Listeria monocytogenes. Immunity 35, 236–248. [PubMed: 21867927]
57. Pelayo R, Hirose J, Huang J, Garrett KP, Delogu A, Busslinger M, and Kincade PW (2005). Derivation of 2 categories of plasmacytoid dendritic cells in murine bone marrow. Blood 105, 4407–4415. [PubMed: 15728131]
58. Lui G, Manches O, Angel J, Molens J-P, Chaperot L, and Plumas J (2009). Plasmacytoid dendritic cells capture and cross-present viral antigens from influenza-virus exposed cells. PLoS One 4, e7111. [PubMed: 19771163]

59. Jung A, Kato H, Kumagai Y, Kumar H, Kawai T, Takeuchi O, and Akira S (2008). Lymphocytoid choriomeningitis virus activates plasmacytoid dendritic cells and induces a cytotoxic T-cell response via MyD88. J. Virol. 82, 196–206. [PubMed: 17942529]
60. Liu X, and Secombe J (2015). The Histone Demethylase KDM5 Activates Gene Expression by Recognizing Chromatin Context through Its PHD Reader Motif. Cell Rep. 13, 2219–2231. [PubMed: 26673323]
61. Liu H, Zhai L, Liu Y, Lu D, Vander Ark A, Yang T, and Krawczyk CM (2023). The histone demethylase KDM5C controls female bone mass by promoting energy metabolism in osteoclasts. Sci. Adv. 9, eadg0731. [PubMed: 37018401]
62. Zorova LD, Popkov VA, Plotnikov EY, Silachev DN, Pevzner IB, Jankauskas SS, Babenko VA, Zorov SD, Balakireva AV, Juhaszova M, et al. (2018). Mitochondrial membrane potential. Anal. Biochem. 552, 50–59. [PubMed: 28711444]
63. Lança T, Ungerbäck J, Da Silva C, Joeris T, Ahmadi F, Vandamme J, Svensson-Frej M, Mowat AM, Kotarsky K, Sigvardsson M, and Agace WW (2022). IRF8 deficiency induces the transcriptional, functional, and epigenetic reprogramming of cDC1 into the cDC2 lineage. Immunity 55, 1431–1447.e11. [PubMed: 35830859]
64. Kurotaki D, Kikuchi K, Cui K, Kawase W, Saeki K, Fukumoto J, Nishiyama A, Nagamune K, Zhao K, Ozato K, et al. (2022). Chromatin structure undergoes global and local reorganization during murine dendritic cell development and activation. Proc. Natl. Acad. Sci. USA 119, e2207009119. [PubMed: 35969760]
65. Leylek R, Alcántara-Hernández M, Granja JM, Chavez M, Perez K, Diaz OR, Li R, Satpathy AT, Chang HY, and Idoyaga J (2020). Chromatin landscape underpinning human dendritic cell heterogeneity. Cell Rep. 32, 108180. [PubMed: 32966789]
66. Mann-Nüttel R, Ali S, Petzsch P, Köhrer K, Alferink J, and Scheu S (2021). The transcription factor reservoir and chromatin landscape in activated plasmacytoid dendritic cells. BMC Genom. Data 22, 37. [PubMed: 34544361]
67. Chauvistré H, Küstermann C, Rehage N, Klisch T, Mitzka S, Felker P, Rose-John S, Zenke M, and Seré KM (2014). Dendritic cell development requires histone deacetylase activity. Eur. J. Immunol. 44, 2478–2488. [PubMed: 24810486]
68. Zhang Y, Wu T, He Z, Lai W, Shen X, Lv J, Wang Y, and Wu L (2023). Regulation of pDC fate determination by histone deacetylase 3. Elife 12, e80477. 10.7554/eLife.80477. [PubMed: 38011375]
69. Yang B, Kim S, Jung W-J, Kim K, Kim S, Kim Y-J, Kim T-G, Lee E-C, Joo J-S, Park CG, et al. (2023). CTCF controls three-dimensional enhancer network underlying the inflammatory response of bone marrow-derived dendritic cells. Nat. Commun. 14, 1277. [PubMed: 36882470]
70. Villar J, and Segura E (2020). Decoding the Heterogeneity of Human Dendritic Cell Subsets. Trends Immunol. 41, 1062–1071. [PubMed: 33250080]
71. Brodin P, and Davis MM (2017). Human immune system variation. Nat. Rev. Immunol. 17, 21–29. [PubMed: 27916977]
72. Granot T, Senda T, Carpenter DJ, Matsuoka N, Weiner J, Gordon CL, Miron M, Kumar BV, Griesemer A, Ho S-H, et al. (2017). Dendritic Cells Display Subset and Tissue-Specific Maturation Dynamics over Human Life. Immunity 46, 504–515. [PubMed: 28329707]
73. Papaioannou NE, Salei N, Rambichler S, Ravi K, Popovic J, Küntzel V, Lehmann CH, Fiancette R, Salvermoser J, Gajdasik DW, et al. (2021). Environmental Signals Rather Than Layered Ontogeny Imprint the Function of Type 2 Conventional Dendritic Cells in Young and Adult Mice. Nat. Commun. 12, 464. 10.1038/s41467-020-20659-2. [PubMed: 33469015]
74. Love MI, Huber W, and Anders S (2014). Moderated estimation of fold change and dispersion for RNA-seq data with DESeq2. Genome Biol. 15, 550. [PubMed: 25516281]
75. Yu G, Wang L-G, Han Y, and He Q-Y (2012). clusterProfiler: an R package for comparing biological themes among gene clusters. OMICS 16, 284–287. [PubMed: 22455463]
76. Li H (2013). Aligning sequence reads, clone sequences and assembly contigs with BWA-MEM. Preprint at arXiv. 10.48550/ar-Xiv.1303.3997.
77. Faust GG, and Hall IM (2014). SAMBLASTER: fast duplicate marking and structural variant read extraction. Bioinformatics 30, 2503–2505. [PubMed: 24812344]

78. Li H, Handsaker B, Wysoker A, Fennell T, Ruan J, Homer N, Marth G, Abecasis G, and Durbin R (2009). 1000 Genome Project Data Processing Subgroup, The Sequence Alignment/Map format and SAMtools. Bioinformatics 25, 2078–2079. [PubMed: 19505943]

79. Zhang Y, Liu T, Meyer CA, Eeckhoute J, Johnson DS, Bernstein BE, Nusbaum C, Myers RM, Brown M, Li W, and Liu XS (2008). Model-based analysis of ChIP-Seq (MACS). Genome Biol. 9, R137. [PubMed: 18798982]

80. Amemiya HM, Kundaje A, and Boyle AP (2019). The ENCODE Blacklist: Identification of Problematic Regions of the Genome. Sci. Rep. 9, 9354. [PubMed: 31249361]

81. Ramírez F, Ryan DP, Grüning B, Bhardwaj V, Kilpert F, Richter AS, Heyne S, Dündar F, and Manke T (2016). deepTools2: a next generation web server for deep-sequencing data analysis. Nucleic Acids Res. 44, W160–W165. [PubMed: 27079975]

82. Zerbino DR, Johnson N, Juettemann T, Wilder SP, and Flicek P (2014). WiggleTools: parallel processing of large collections of genome-wide datasets for visualization and statistical analysis. Bioinformatics 30, 1008–1009. [PubMed: 24363377]

83. Ross-Innes CS, Stark R, Teschendorff AE, Holmes KA, Ali HR, Dunning MJ, Brown GD, Gojis O, Ellis IO, Green AR, et al. (2012). Differential oestrogen receptor binding is associated with clinical outcome in breast cancer. Nature 481, 389–393. [PubMed: 22217937]

84. Yu G, Wang L-G, and He Q-Y (2015). ChIPseeker: an R/Bioconductor package for ChIP peak annotation, comparison and visualization. Bioinformatics 31, 2382–2383. [PubMed: 25765347]

85. Heinz S, Benner C, Spann N, Bertolino E, Lin YC, Laslo P, Cheng JX, Murre C, Singh H, and Glass CK (2010). Simple combinations of lineage-determining transcription factors prime cis-regulatory elements required for macrophage and B cell identities. Mol. Cell 38, 576–589. [PubMed: 20513432]

86. Iwase S, Brookes E, Agarwal S, Badeaux AI, Ito H, Vallianatos CN, Tomassy GS, Kasza T, Lin G, Thompson A, et al. (2016). A Mouse Model of X-linked Intellectual Disability Associated with Impaired Removal of Histone Methylation. Cell Rep. 14, 1000–1009. [PubMed: 26804915]

87. Kirkling ME, Cytlak U, Lau CM, Lewis KL, Resteu A, Khodadadi-Jamayran A, Siebel CW, Salmon H, Merad M, Tsirigos A, et al. (2018). Notch Signaling Facilitates In Vitro Generation of Cross-Presenting Classical Dendritic Cells. Cell Rep. 23, 3658–3672.e6. [PubMed: 29925006]

88. Stephens M (2017). False discovery rates: a new deal. Biostatistics 18, 275–294. [PubMed: 27756721]

89. Skene PJ, and Henikoff S (2017). An efficient targeted nuclease strategy for high-resolution mapping of DNA binding sites. Elife 6, e21856. 10.7554/eLife.21856. [PubMed: 28079019]

90. Zhang Z, Hernandez K, Savage J, Li S, Miller D, Agrawal S, Ortuno F, Staudt LM, Heath A, and Grossman RL (2021). Uniform genomic data analysis in the NCI Genomic Data Commons. Nat. Commun. 12, 1226. [PubMed: 33619257]

91. Wilson SL, Shen SY, Harmon L, Burgener JM, Triche T Jr., Brat-man SV, De Carvalho DD, and Hoffman MM (2022). Sensitive and reproducible cell-free methylome quantification with synthetic spike-in controls. Cell Rep. Methods 2, 100294. [PubMed: 36160046]

Highlights

- KDM5C regulates pDC and cDC heterogeneity
- Ly6C^{-} pDCs are poor producers of IFN-α but can present antigens to CD8 T cells
- KDM5C antagonizes IRF-driven gene expression, increasing baseline activation of pDC and cDC1
- KDM5C is required for functional responses of pDCs and cDC1s

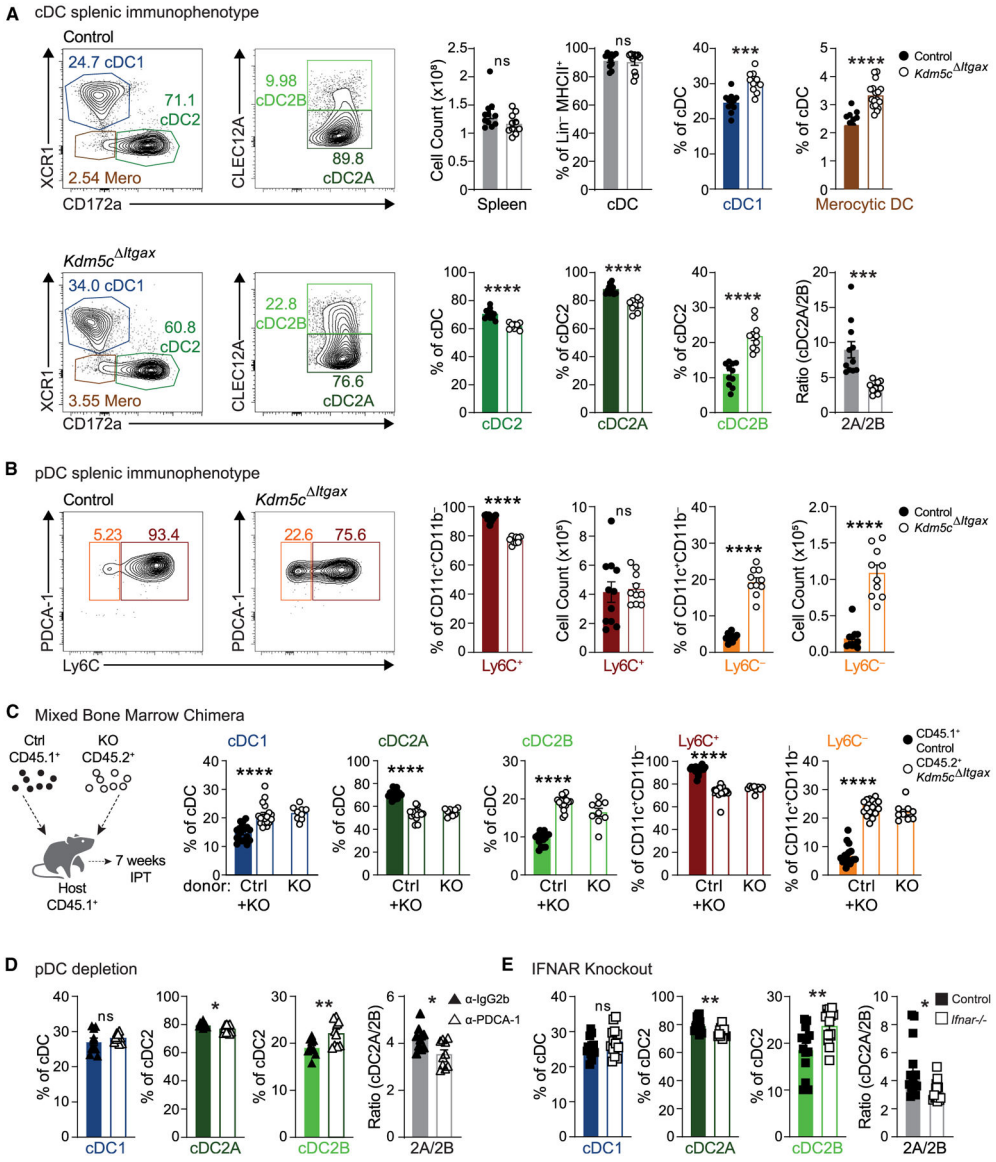

Figure 1. KDM5C regulates cDC and pDC heterogeneity

(A) Representative plots and frequencies of splenic XCR1$^+$ cDC1s, XCR1$^-$CD172a$^-$ merocytic DCs (mero), CLEC12A$^-$ cDC2A, and CLEC12A$^+$ cDC2B of total cDCs (Lin$^-$MHCII$^+$CD11c$^+$CD26$^+$) or of total cDC2s (CD172a$^+$) in female control (top) and *Kdm5c*$^{\Delta Itgax}$ (bottom) mice.

(B) Representative plots, proportions, and counts of splenic Ly6C$^+$ pDCs and Ly6C$^-$ pDCs from female control and *Kdm5c*$^{\Delta Itgax}$ mice (parent gate: Lin(B220)$^+$SiglecH$^+$CD11c^{int}CD11b$^-$).

(C) BM chimeras were generated in CD45.1$^+$ host mice by reconstituting their BM with a 1:1 mixture of CD45.1$^+$ control and CD45.2$^+$ *Kdm5c*$^{\Delta Itgax}$ BM or CD45.2$^+$ *Kdm5c*$^{\Delta Itgax}$ BM alone. Proportions of splenic DC subsets are derived from CD45.1$^+$ control and CD45.2$^+$ *Kdm5c*$^{\Delta Itgax}$ cells 7 weeks post injection.

(D) Proportions of splenic cDCs of mice administered α-IgG2b or α-PDCA1 to deplete pDCs.

(E) Frequencies of splenic cDCs from control and *Ifnar1*$^{-/-}$ mice. Each symbol represents an individual mouse. Data were pooled from 2–3 experiments of 9–11 mice per group. (A, B, D, and E) Statistical significance was determined by unpaired t test or (C) one-way ANOVA. *$p < 0.05$, **$p < 0.01$, ***$p < 0.001$, ****$p < 0.0001$. All error bars represent mean and SEM. See also Figure S1.

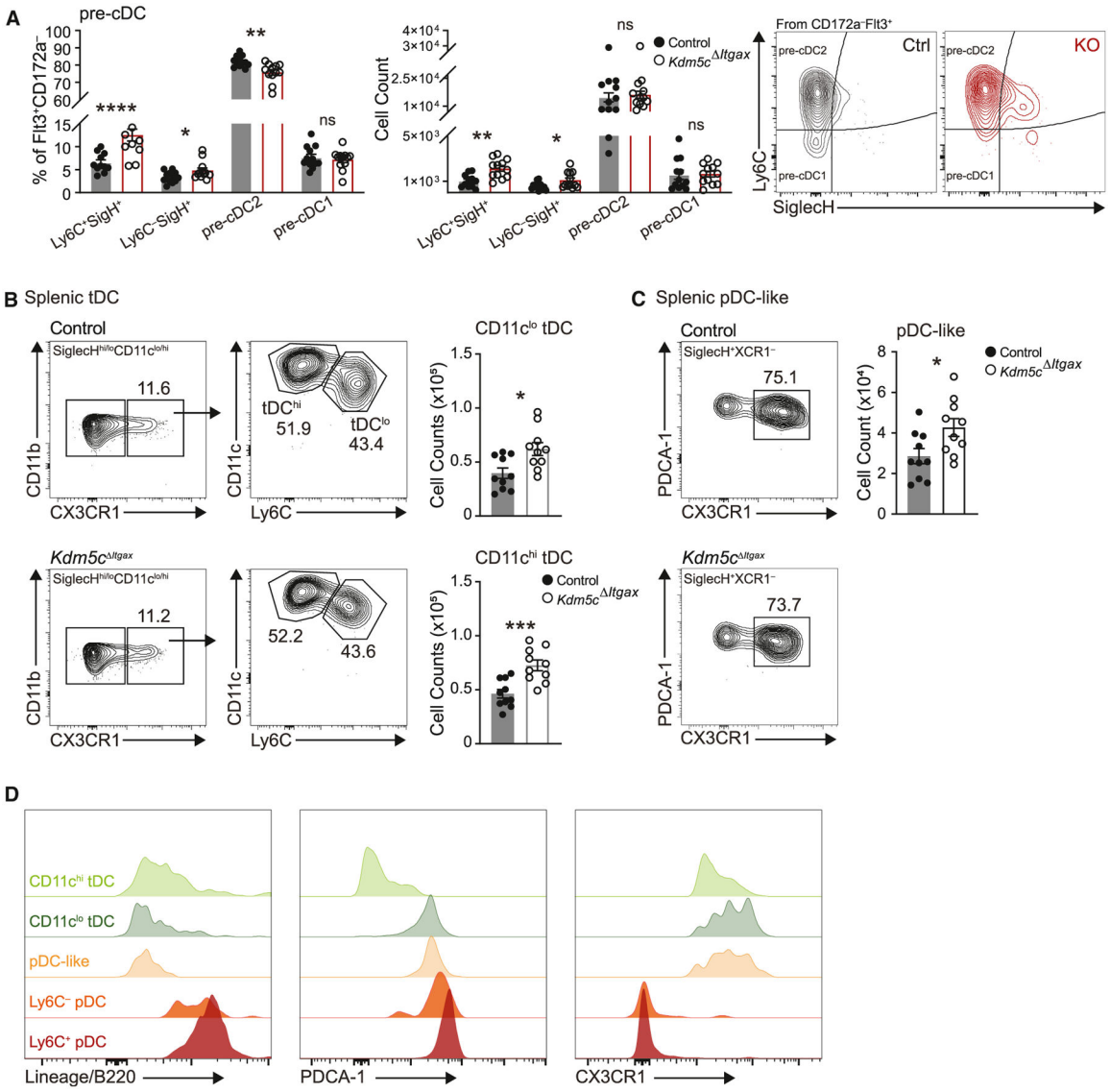

Figure 2. Ly6C− pDCs are distinct from tDC, pDC-like, and DC precursors

(A–C) Evaluation of (A) pre-DC, (B) tDC, and (C) pDC-like cells in the BM using gating strategies described in Figure S2.

(D) Histograms of indicated surface proteins of tDC, pDC-like cells compared with Ly6C^{-} and Ly6C^{+} pDC. Each symbol represents an individual mouse. (A–C) Data were pooled from 3 or more experiments with (A) 12 mice per group and (B and C) 10 mice per group. (D) Data are of one experiment representative of three or more experiments. Statistical significance was determined by (B and C) unpaired t test or (A) one-way ANOVA. *$p <$ 0.05, **$p < 0.01$, ****$p < 0.001$. All error bars represent mean and SEM. See also Figure S2.

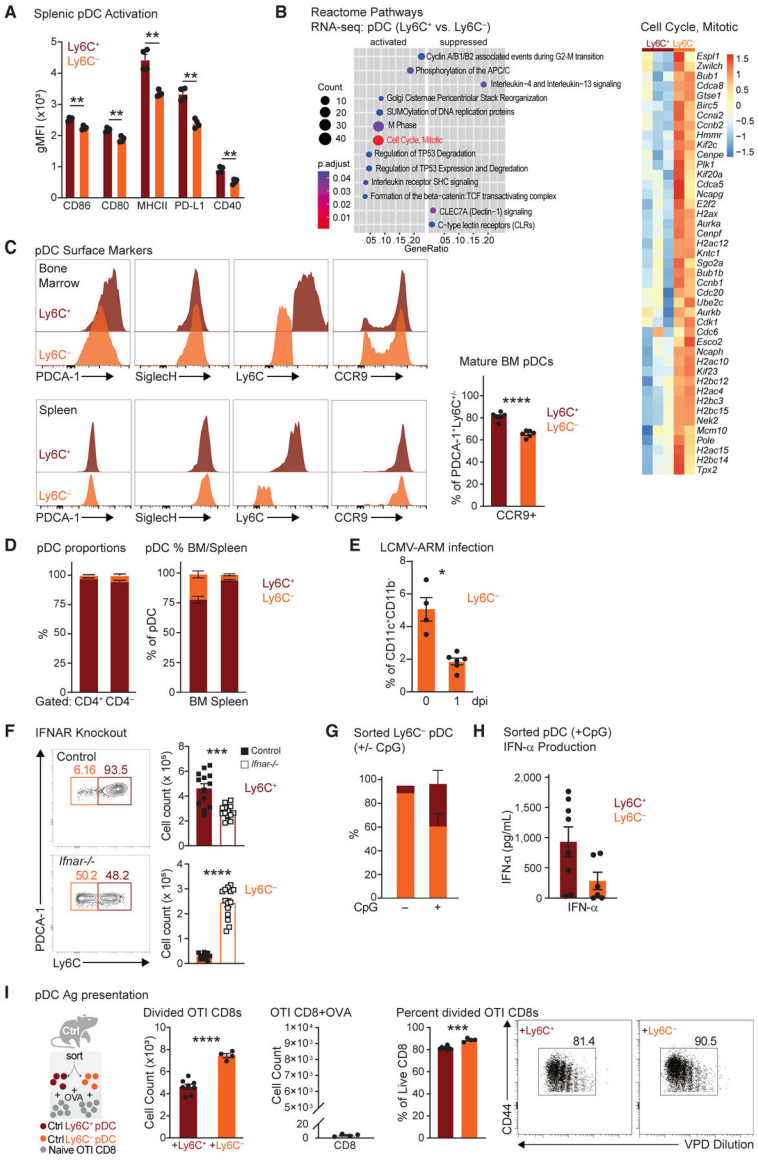

Figure 3. Ly6C− and Ly6C+ pDCs are functionally distinct

(A) Geometric mean fluorescence intensity (gMFI) of activation markers expressed by Ly6C$^+$ and Ly6C$^-$ pDCs.

(B) GSEA of DEGs (false discovery rate [FDR] of <0.01) (left) between Ly6C$^+$ and Ly6C$^-$ pDCs and heatmap of significant cell cycle DEGs (FDR of <0.05) (right).

(C) Histograms of PDCA-1, SiglecH, Ly6C, and CCR9 expression of Ly6C$^+$ and Ly6C$^-$ pDCs from bone marrow (top) and spleen (bottom). Frequency of CCR9$^+$ cells in Ly6C$^+$ and Ly6C$^-$ pDCs in BM (right).

(D) Proportions of Ly6C$^+$ and Ly6C$^-$ pDCs as a percentage of CD4$^+$ and CD4$^-$ pDCs (left) and in the BM and spleen (right).

(E) Proportions of splenic Ly6C$^-$ pDCs at steady state and 20 h post infection with LCMV-ARM.

(F) Cell counts of splenic Ly6C$^+$ pDCs and Ly6C$^-$ pDCs from control and *Ifnar1*$^{-/-}$ mice.

(G) Percentages of Ly6C$^+$ and Ly6C$^-$ pDCs after CpG stimulation of sorted Ly6C$^-$ pDCs.
(H) IFN-α production by sorted splenic Ly6C$^+$ and Ly6C$^-$ pDCs stimulated with TLR9 ligand CpG ODN 1585 for 18 h, measured by ELISA.
(I) Ly6C$^+$ and Ly6C$^-$ pDCs sorted from control mice were incubated with OVA and co-cultured with naive OTI CD8 T cells. Cell counts and percentage of divided OTI CD8 T cells after co-culture with pDCs or with OVA alone. Representative plots of CD44 by violet proliferation dye (VPD) show gates of divided OTI CD8 T cells. Data shown in (A) are of one experiment representative of more than three experiments and error bars represent mean and SEM of four mice per group, (C) pooled from two experiments (mean and SEM of 6 mice per group), (E) one experiment representative of more than three experiments (mean and SEM of 4 or 5 mice per group), (F) pooled from three experiments (mean and SEM of 14 mice per group), (G) one experiment with four technical replicates; mean and SD (H) pooled from two experiments (mean and SEM of 8 and 6 mice per group), or (I) of one experiment representative of two experiments (mean and SEM of 8 Ly6C$^+$ and 4 Ly6C$^-$ pDC replicates). Statistical significance was determined for (C, E, F, H, I) by unpaired t test and (A) multiple unpaired t test. *$p < 0.05$, **$p < 0.01$, ***$p < 0.001$, ****$p < 0.0001$. See also Figure S3.

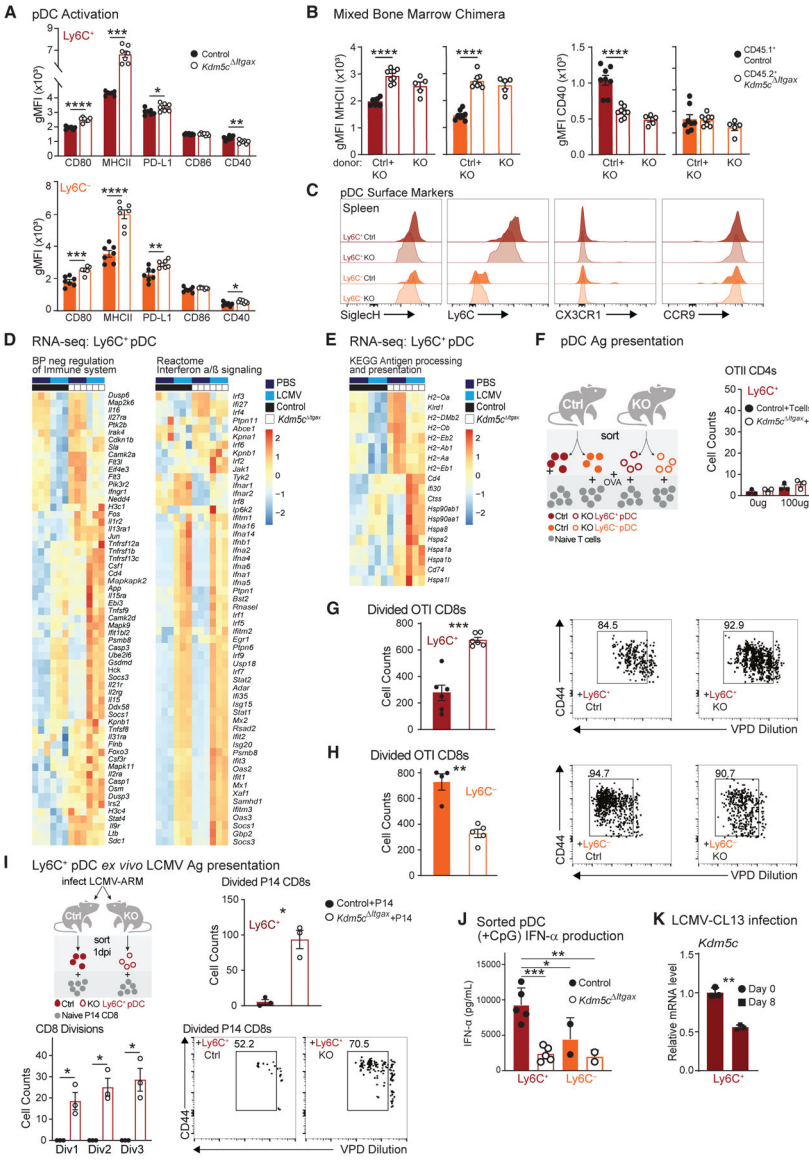

Figure 4. KDM5C promotes pDC function

(A) Geometric mean fluorescence intensity (gMFI) of activation markers of Ly6C$^+$ and Ly6C$^-$ pDCs from control or *Kdm5c*$^{\Delta Itgax}$ mice.

(B) Bone marrow chimeras as in Figure 1D, and gMFI of MHC II and CD40 expressed by splenic cDC subsets derived from CD45.1$^+$ control and CD45.2$^+$ *Kdm5c*$^{\Delta Itgax}$ cells 7 weeks post injection.

(C) Histograms of SiglecH, Ly6C, CX3CR1, and CCR9 expression by splenic Ly6C$^+$ and Ly6C$^-$ pDCs from control and *Kdm5c*$^{\Delta Itgax}$ mice.

(D) Heatmap of significantly different genes (false discovery rate of <0.05) between *Kdm5c*$^{\Delta Itgax}$ Ly6C$^-$ and Ly6C$^+$ pDCs with or without LCMV infection (20 h) of indicated pathways.

(E) Heatmap of DEGs from Kyoto Encyclopedia of Genes and Genomes (KEGG) pathways on antigen processing and presentation of control and *Kdm5c*$^{\Delta itgax}$ Ly6C^{+} pDCs from mice with or without LCMV infection.

(F) Ly6C^{+} and Ly6C^{-} pDCs were sorted from control and *Kdm5c*$^{\Delta Itgax}$ spleens, incubated with or without 100 μg OVA, and cultured with naive OTI CD8 or OT-II CD4 T cells for 3 days. Cell counts of OT-II CD4 co-cultured with Ly6C^{+} pDCs (right).

(G and H) Cell counts of OTI CD8 T cells and representative plots of violet proliferation dye (VPD) by CD44 of OTI CD8 T cells after co-culture with (G) Ly6C^{+} pDCs and (H) Ly6C^{-} pDCs.

(I) Ly6C^{+} pDC were sorted from control and *Kdm5c*$^{\Delta Itgax}$ mice 1 dpi with LCMV-ARM and co-cultured with P14 CD8 T cells for 3 days. Cell counts for total divided P14 CD8 T cells (top right) and for each division (bottom left). Representative plots of CD44 by VPD with gates on divided P14 CD8 T cells.

(J) IFN-α production by sorted pDC subsets from control and *Kdm5c*$^{\Delta Itgax}$ mice stimulated with TLR9 ligand CpG ODN 1585 for 18 h (ELISA).

(K) qPCR of *Kdm5c* from sorted splenic Ly6C^{+} pDCs at steady state and 8 dpi with LCMV-CL13. Data are of (A, B) one experiment representative of two to five experiments (mean and SEM of 3–8 mice per experiment), (F–H) one experiment representative of two experiments (mean and SEM of 4–6 replicates per group), (I) one experiment representative of two experiments (mean and SEM of 3 per group), (J) sorted DCs pooled from three control and *Kdm5c*$^{\Delta Itgax}$ mice mean and SD and (K) pooled RNA from sorted pDC from six mice run in triplicate (mean and SEM). Statistical significance was determined by (H and K) unpaired t test, (A and I) multiple unpaired t test, or (B and J) one-way ANOVA. See also Figure S4.

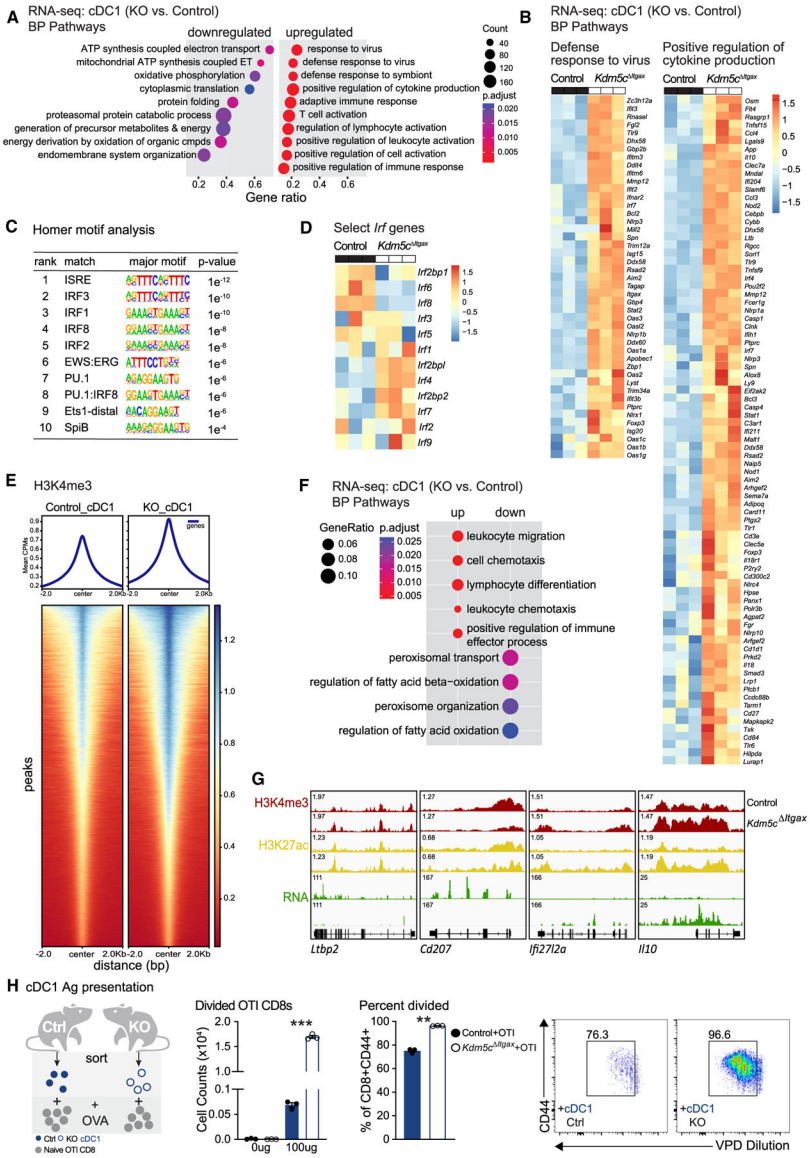

Figure 5. KDM5C regulates inflammatory gene expression in cDC1

(A and B) Pathway analyses (A) and heatmaps (B) of DEGs between KDM5C-deficient (*Kdm5c*$^{\Delta Itgax}$) and control cDC1.

(C) Enriched TF motifs in promoters of genes with increased expression in the absence of KDM5C.

(D) Heatmap of *Irf* genes.

(E) Heatmaps of H3K4me3 (CUT&RUN) segregated by direction of differential expression.

(F) Pathway analysis of genes with differentially methylated regions.

(G) IGV tracks showing H3K4me3, H3K27Ac, and RNA expression (RNA-seq).

(H) cDC1s were sorted from control and *Kdm5c*$^{\Delta Itgax}$ mice, incubated with OVA, and co-cultured with naive OTI CD8 T cells. Cell counts and percentage of divided OTI CD8 T cells represented in CD44 by VPD plots. Data shown in (A–G) are from three biological replicates of each genotype. Data in (H) are of one experiment representative of two

experiments (mean and SEM of 3 per group). Statistical significance was determined by (H) unpaired t test. $^{**}p < 0.01$, $^{***}p < 0.001$. See also Figure S5.

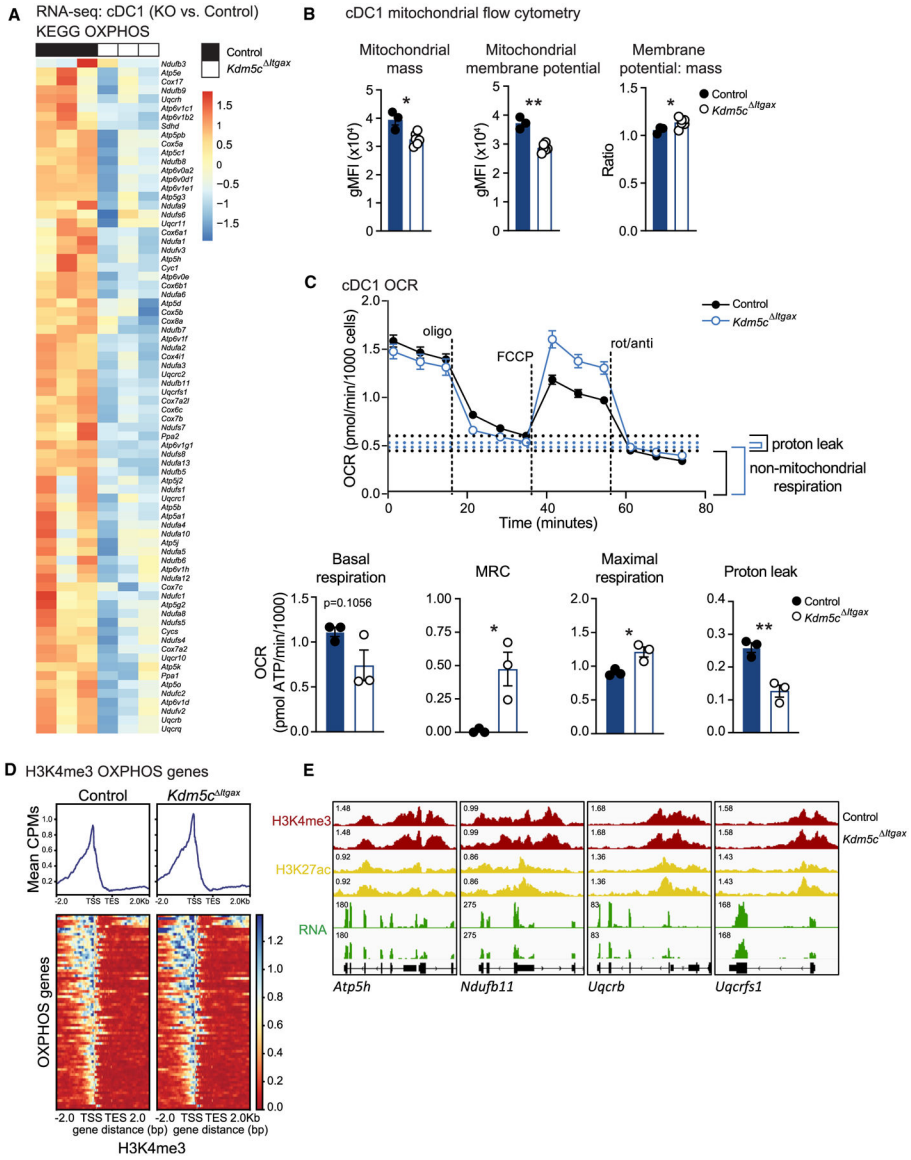

Figure 6. KDM5C regulates OXPHOS gene expression and mitochondrial function in cDC1

(A) Heatmap of DEGs encoding factors from Kyoto Encyclopedia of Genes and Genomes (KEGG) OXPHOS pathway by splenic cDC1 from control and *Kdm5c*$^{\Delta Itgax}$ mice.

(B) Geometric mean fluorescence intensity (gMFI) of MitoSpy Green (mitochondrial mass) and TMRM (mitochondrial membrane potential), and ratio of mitochondrial membrane potential to mass.

(C) OCR per 1,000 cells measured over time of sorted control and *Kdm5c*$^{\Delta Itgax}$ cDC1 sequentially treated by oligomycin, FCCP, and rotenone/antimycin A. Basal respiration (OCR of cells without drug treatment), MRC (maximal respiration minus basal respiration), maximal respiration (OCR after FCCP treatment), and proton after (OCR following oligomycin treatment minus OCR after rotenone/antimycin A treatment).

(D) Heatmap of H3K4me3 of genes shown in (A).

(E) IGV tracks showing H3K4me3, H3K27Ac, and RNA expression (RNA-Seq). Data shown in (A, D, and E) are three biological replicates per group. Data are of one experiment representative of (B) two experiments (mean and SEM of 3 control and 6 *Kdm5c*$^{\Delta Itgax}$ mice), (C) two experiments (mean and SEM of 3 replicates). Statistical significance in (B and C) were determined by unpaired t test. *$p < 0.05$, **$p < 0.01$. See also Figure S6.

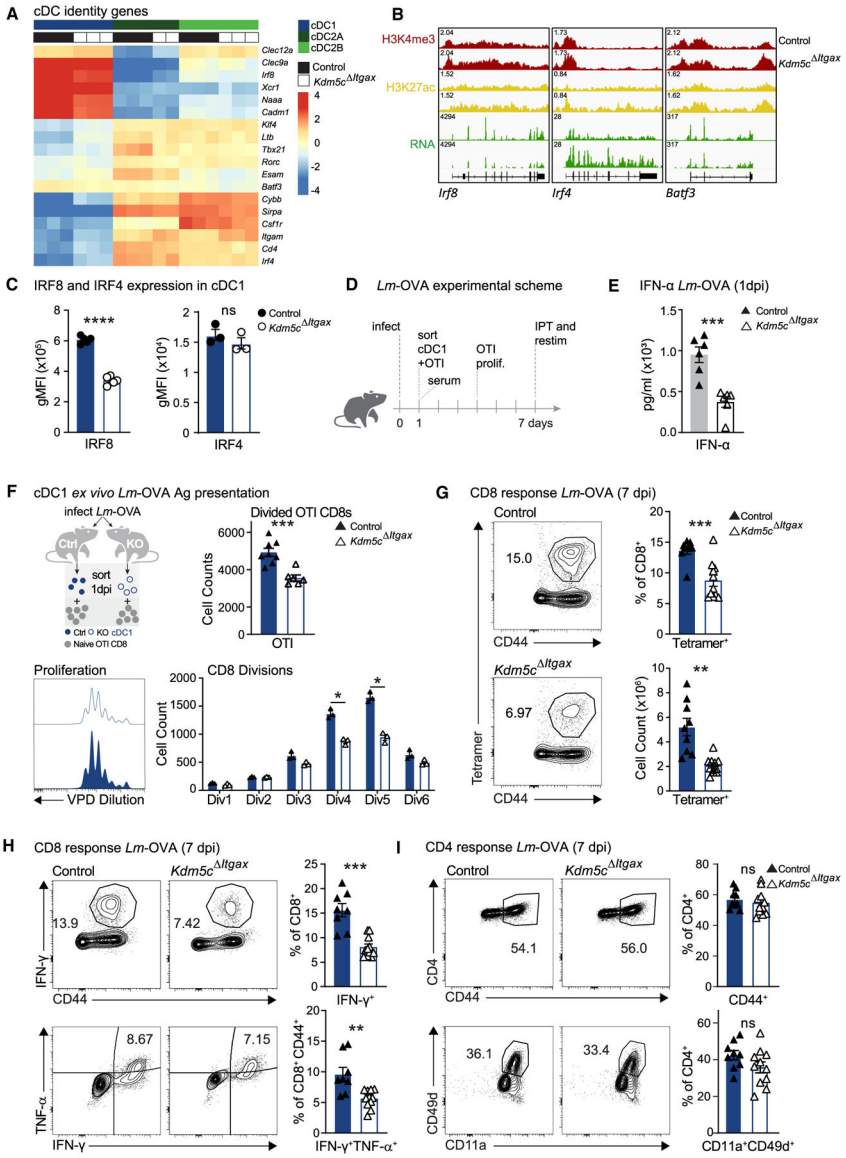

Figure 7. KDM5C expression in DCs is required for lineage-specific gene expression and DC function during infection

(A) Heatmap of gene expression of markers specific to cDC subsets by cDC1, cDC2A, and cDC2B sorted from control and *Kdm5c*$^{\Delta Itgax}$ splenocytes.

(B) IGV tracks showing H3K4me3, H3K27Ac, and RNA expression (RNA-seq).

(C) Geometric mean fluorescence intensity (gMFI) of IRF8 and IRF4 in control and *Kdm5c*$^{\Delta Itgax}$ splenic cDC1.

(D) Experimental scheme showing infection of control and *Kdm5c*$^{\Delta Itgax}$ mice with *Lm*-OVA for (E and F) 1 day or (G–I) 7 days. (E) Serum IFN-α levels. (F) Sorted cDC1 1 dpi were cultured with naive OTI CD8 T cells and T cell proliferation was assessed by comparing the number of total divided OTI CD8 T cells (top right) and the number of CD8 T cells at each division (bottom). The frequencies of (G) OVA-specific (tetramer$^+$) cells of CD8 T cells, and (H) IFN-γ$^+$ of CD8$^+$ T cells (top) and IFN- γ$^+$ tumor necrosis factor (TNF)-α$^+$ polyfunctional cells of CD8$^+$CD44$^+$ T cells (bottom). (I) CD44$^+$ (top) and CD11a$^+$CD49d$^+$

(bottom) of CD4 T cells. Data in (A) are of three biological replicates per group except for *Kdm5c*$^{\Delta Itgax}$ cDC2B with two biological replicates, (C) one experiment representative of two (mean and SEM 5 mice per group IRF8; or 3 per group IRF4), (E) are of two pooled experiments (mean and SEM of 6 mice per group). Data in (F) are of one experiment representative of three experiments (mean and SEM of 8 control and 6 *Kdm5c*$^{\Delta Itgax}$ mice; significance determined by multiple unpaired t tests. Data in (G–I) are pooled from two experiments (mean and SEM of 8 control and 11 *Kdm5c*$^{\Delta Itgax}$ mice). Statistical significance in (C, E, G–I) were determined by unpaired t test. *$p < 0.05$, **$p < 0.01$, ***$p < 0.001$. See also Figure S7.

KEY RESOURCES TABLE

REAGENT or RESOURCE	SOURCE	IDENTIFIER
Antibodies		
Anti-mouse CD86 BUV395 (clone GL1)	BD Biosciences	564199; RRID:AB_2738664
Anti-mouse CD11c BUV737 (clone N418 (RUO))	BD Biosciences	749039; RRID:AB_394034
Anti-mouse CLEC12A BV421 (clone 5D3/CD371)	BD Biosciences	564795; RRID:AB_11154053
Anti-mouse CD317 Pac Blue (clone 927)	Biolegend	127018; RRID:AB_2259316
Anti-mouse CD11b BV570 (clone M1/70)	Biolegend	101233; RRID:AB_11150781
Anti-mouse I-A/I-E BV605 (clone M5/114.15.2)	Biolegend	107639; RRID:AB_2565894
Anti-mouse XCR1 BV650 (clone ZET)	Biolegend	148220; RRID:AB_2566410
Anti-mouse Ly6C BV711 (HK1.4)	Biolegend	128037; RRID:AB_2562630
Anti-mouse CD40 SB780 (clone 1C10)	eBioscience	78-0401-82; RRID:AB_2762674
Anti-mouse CX3CR1 PE (clone SA011F11)	Biolegend	149006; RRID:AB_2564314
Anti-mouse F4/80 PE/Dazzle 594 (clone BM8)	Biolegend	123146; RRID:AB_2564133
Anti-mouse CD274 PE/Cy7 (clone 10F.9G2)	Biolegend	124314; RRID:AB_10643573
Anti-mouse CD64 PerCp/Cy5.5 (clone X54–5/7.1)	Biolegend	139308; RRID:AB_2561963
Anti-mouse CD26 APC (clone H194–112)	Biolegend	137807; RRID:AB_10663403
Anti-mouse CD172a AF700 (clone P84)	Biolegend	144022; RRID:AB_2650813
Anti-mouse Siglec-H APC/Vio 770 (clone REA819)	Miltenyi	130-112-299; RRID:AB_2653464
Anti-mouse Ly6G FITC (clone 1AB-Ly6g)	eBioscience	11-9668-82; RRID:AB_2572532
Anti-mouse B220 FITC (clone RA3–6B2)	eBioscience	11-0452-82; RRID:AB_465054
Anti-mouse CD3 FITC (clone 17A2)	eBioscience	11-0032-82; RRID:AB_2572431
Anti-mouse CD19 FITC (clone 1D3)	eBioscience	11-0193-85; RRID:AB_657668
Anti-mouse NK1.1 FITC (clone PK136)	Biolegend	11-5941-82; RRID:AB_465318
Anti-mouse CLEC12A APC (clone 5D3)	Biolegend	143405; RRID:AB_2564264
Anti-Mouse XCR1 APC/Cy7 (clone ZET)	Biolegend	148224; RRID:AB_2783118
Anti-mouse CD64 FITC (clone X54–5/7.1)	Biolegend	139316; RRID:AB_2566556
Anti-mouse CD11b PerCp/Cy5.5 (clone M1/70)	eBioscience	45-0112-80; RRID:AB_953560
Anti-mouse CD11c PE/Cy7 (clone N418)	eBioscience	25-0114-82; RRID:AB_469590
Anti-mouse CD317 BV421 (clone 927)	Biolegend	127023; RRID:AB_2687109
Anti-mouse B220 BV650 (clone RA3–6B2)	Biolegend	103241; RRID:AB_11204069
Anti-mouse Ly6C PE (clone HK1.4)	eBioscience	12-5932-82; RRID:AB_10804510
Anti-mouse CD62L BUV395 (clone MEL-14)	BD Biosciences	740218; RRID:AB_2739966
Anti-mouse CD4 BUV496 (clone RM4–5)	BD Biosciences	741050; RRID:AB_2870665
Anti-mouse KLRG1 BUV661 (clone 2F1)	BD Biosciences	741586; RRID:AB_2870999
Anti-mouse CD8a BUV805 (clone 53–6.7)	BD Biosciences	612898; RRID:AB_2870186
Anti-mouse CD223 e450 (clone C9B7W)	eBioscience	48-2231-80; RRID:AB_11151690
Anti-mouse CD279 BV605 (clone 29F.1A12)	Biolegend	135219; RRID:AB_11125371
Anti-mouse CD44 BV650 (clone 1M7)	Biolegend	103049; RRID:AB_2562600
Anti-mouse CD127 BV785 (clone A7R34)	Biolegend	135037; RRID:AB_2565269
Anti-mouse CD3e PerCP/Cy5.5 (clone 145–2C11)	eBioscience	45-0031-82; RRID:AB_1107000
Kb/OVA257 PE Tetramer	Baylor College of Medicine	20067

REAGENT or RESOURCE	SOURCE	IDENTIFIER
Anti-mouse CD49 d PE/Dazzle 594 (clone R1–2)	Biolegend	103626; RRID:AB_2734161
Anti-mouse CD11a PE/Cy7 (clone M17/4)	Biolegend	101122; RRID:AB_2562781
Anti-mouse CD25 APC (clone PC61.5)	eBioscience	17-0251-82; RRID:AB_469366
Anti-mouse KLRG1 AF532 (clone 2F1)	eBioscience	58-5893-80; RRID:AB_281528
Anti-mouse CX3CR1 AF700 (clone SA011F11)	Biolegend	149036; RRID:AB_2629606
Anti-mouse CD8a APC/efluor780 (clone 53–6.7)	eBioscience	47-0081-82; RRID:AB_1272185
Anti-mouse CD44 BUV805 (clone IM7)	BD Biosciences	741921; RRID:AB_2871234
Anti-mouse CD69 BUV496 (clone H1.2F3)	BD Biosciences	741063; RRID:AB_2870675
Anti-mouse LY108 PacBlue (clone 330-AJ)	Biolegend	134608; RRID:AB_2188093
Anti-mouse CD366 BV711 (clone RMT3–23)	Biolegend	119727; RRID:AB_2716208
Anti-mouse CD279 BUV737 (clone RMPI-30)	BD Biosciences	749306; RRID:AB_2873680
Anti-mouse CD4 PE/Cy5 (clone RM4–5)	eBioscience	15-0042-83; RRID:AB_468699
Anti-human/mouse/rat IFNg FITC (clone XMG1.2)	eBioscience	11-7311-82; RRID:AB_465412
Anti-human/mouse TNFa PE/Cy7 (clone MP6-XT22)	eBioscience	25-7321-82; RRID:AB_11042728
Anti-human/mouse Tox PE (clone REA473)	Miltenyi	130-120-785; RRID:AB_2801785
Anti-human/mouse TCF1/TCF7 AF647 (clone C63D9)	Cell Signaling	6709; RRID:AB_2797631
Anti-human/mouse Granzyme B PE/Dazzle 594 (clone QA16A02)	Biolegend	372216; RRID:AB_2728383
Anti-human/mouse T-bet BV605 (clone 4B10)	Biolegend	644817; RRID:AB_11219388
anti-KDM5C antibody EPR18653	Abcam	Ab194288
*In Vivo*MAb anti-mouse CD317 (clone 927)	BioXcell	BE0311; RRID:AB_2736991
*In Vivo*MAb rat IgG2b isotype control (clone LTF-2)	BioXcell	BE0090; RRID:AB_1107780
anti-β-actin antibody	Cell Signaling	4967S; RRID:AB_330288
Anti-rabbit IgG, HRP-linked Antibody	Cell Signaling	7074S; RRID:AB_2099233
Anti-mouse CD317 APC (clone 927)	eBiosceince	17-3172-82; RRID:AB_10596356
Anti-mouse B220 PerCP/Cy5.5 (clone RA3-6B2)	eBioscience	45-0452-82; RRID:AB_1107006
Anti-mouse CD11b APC/Cy7 (clone M1/70)	eBioscience	47-0112-82; RRID:AB_1603193
Anti-mouse CD8a APC (clone 53-6.7)	eBioscience	17-0081-83; RRID:AB_469336
Anti-mouse CD8 BUV395 (clone 53–6.7)	BD Biosciences	563786; RRID:AB_2732919
Anti-mouse B220 BUV661 (clone RA3–6B2)	BD Biosciences	565077; RRID:AB_2739056
Anti-mouse CD135 BV421 (clone A2F10)	Biolegend	135315; RRID:AB_2571919
Anti-mouse CD24 PacBlue (clone M1/69)	Biolegend	101820; RRID:AB_572010
Anti-mouse CD117 BV605 (clone 2B8)	Biolegend	105847; RRID:AB_2783047
Anti-mouse CD45 BV785 (clone 30-F11)	Biolegend	103149; RRID:AB_2564590
Anti-mouse CD172a PerCP/e710 (clone P84)	eBioscience	46-1721-82; RRID:AB_10804639
Anti-mouse Ly6D PE (clone 49-H4)	Biolegend	138603; RRID:AB_2137349
Anti-mouse CD115 PE/Dazzle 594 (clone AFS98)	Biolegend	135528; RRID:AB_2566522
Anti-mouse CD127 PE/Cy7 (clone A7R34)	eBioscience	25-1271-82; RRID:AB_469649
Anti-mouse CX3CR1 APC (clone SA011F11)	Biolegend	149008; RRID:AB_2564492
Anti-mouse I-A/I-E AF700 (clone M5/114.15.2)	Biolegend	107622; RRID:AB_493727
Anti-mouse TER119 FITC (clone TER-119)	Biolegend	116206; RRID:AB_313707
Anti-mouse F4/80 FITC (clone BM8)	Biolegend	123108; RRID:AB_893502
Anti-mouse CD45.1 BV785 (clone A20)	Biolegend	110743; RRID:AB_2563379

REAGENT or RESOURCE	SOURCE	IDENTIFIER
Anti-mouse CD45.2 BUV805 (clone 104)	BD Bioscience	741957; RRID:AB_2871265
Anti-mouse CD16/32, non-conjugated Fc Block (clone 93)	eBioscience	14-0161-85; RRID:AB_467134
Anti-mouse CD317 (BDST2/PDCA-1) BV650	Biolegend	127019; RRID:AB_2562477
Anti-mouse CD199 (CCR9) PE	Biolegend	128709; RRID:AB_1227479
Bacterial and virus strains		
LCMV-ARMSTRONG	John T Harty Lab, Iowa	N/A
*Lm*OVA	John T Harty Lab, Iowa	N/A
Chemicals, peptides, and recombinant proteins		
Fixable Viability Dye eFluor™ 780	eBioscience	65-0865-14
eFluor 506 Fixable Viability Dye	ThermoFisher	65-0866-14
Recombinant murine IL-2	Peprotech	212-12
Brefeldin A Solution (100X)	Biolegend	420601
$OVA^{257–264}$ Peptide Fragment	Anaspec	AS-60193-1
cOmplete Mini EDTA-free Protease Inhibitor Cocktail	Roche	11836170001
FLT3L	Peprotech	250-31L
CHAPS lysis buffer	Cell Signaling	9852S
IFN-β	PBL Interferon Source	12410-1
Penicillin-Streptomycin	Gibco	15140122
RPMI 1640	Corning	15-040-CV
ELISA IFN-α	Invitrogen	BMS6027
CpGODN 1585	Invivogen	tlr-kit9m
DNase I recombinant, RNase-free	Roche	04716728001
2-Mercaptoethanol	Gibco	21985023
L-glutamine	Life Technologies	25030081
Tetramethylrhodamine, Methyl Ester, Perchlorate (TMRM)	ThermoFisher Scientific	T668
MitoSpy Green	BioLegend	424806
10X Permeabilization Buffer	eBioscience	00-8333-56
IC fixation buffer	eBioscience	00-8222-49
Collagenase D	Roche	11088858001
HBSS (with Ca^{2+} and Mg^{2+})	Gibco	14025092
IMDM	Gibco	12440-053
NuSerum IV (FBS)	Corning	CB55004
Hoescht stain	ThermoFisher Scientific (Invitrogen)	H21486
DAPI (4’,6-Diamidino-2-Phenylindole, Dihydrochloride)	Invitrogen	D1306
ELISA MAX IFN-a1	Biolegend	447904
Laemmli sample buffer	BioWorld	10570021
Bovine Serum Albumin	Sigma	A7906-50G
SuperSignal™ West Dura Extended Duration Substrate	ThermoFisher	34075
Enrofloxacin	MedChemExpress	HY-B0502S
Tryptic Soy Broth	Millipore Sigma	T8907
Antimycin A	Millipore Sigma	A8674

REAGENT or RESOURCE	SOURCE	IDENTIFIER
Rotenone	Millipore Sigma	R8875
7-AAD Viability Staining Solution	eBioscience	00-6993-50
Critical commercial assays		
Pan Dendritic Cell Isolation Kit, mouse	Miltenyi	130-100-875
XF Cell Mito Stress Test and Seahorse XFe96 Analyzer	Agilent	103015-100
Nextera XT DNA Library preparation kit	Illumina	15032354
AMPure XP SPRI Reagent	Beckman Coulter	A63881
Single Cell RNA Purification kit	Norgen Biotek	51800
Qubit RNA HS Assay Kit	invitrogen	Q32852
Takara SMARTer Stranded total RNA-seq Kit v3	TaKaRa Bio	634487
Qubit HS DNA Assay kit	Invitrogen	Q33230
High Sensitivity DNA Kit	Agilent	5067-4626
Deposited data		
Bulk RNA-seq	This manuscript	GEO: GSE262866
CUT&RUN	This manuscript	GEO: GSE263076
Experimental models: Cell lines		
OP9-DL1 cells	Boris Reizis laboratory	N/A
Experimental models: Organisms/strains		
Mouse: C57BL/6J	Jackson Laboratory	RRID:IMSR_JAX:000664
Mouse: *Ifnar*$^{-/-}$:B6.129S2-*Ifnar1*^{tm1ABt}/Mmjax	Jackson Laboratory	RRID:MMRRC_032045-JAX
Zbtb-Cre: B6.Cg-*Zbtb46*$^{tm3.1(cre)Mnz}$/J	Jackson Laboratory	RRID:IMSR_JAX:028538
Itgax-Cre: B6.Cg-Tg(Itgax-cre)1-1Reiz/J	Jackson Laboratory	RRID:IMSR_JAX:008068
Ly5.1: B6.SJL-*Ptprc*^{a}*Pepc*^{b}/BoyJ	Jackson Laboratory	RRID:IMSR_JAX:002014
Kdm5c-fl/fl	Laboratory of Dr. Y. Shi	N/A
Kdm5c$^{\Delta ItBax}$ (*Kdm5c*-fl/fl x *Itgax*-Cre)	This manuscript	N/A
Kdm5c$^{\Delta Zbtb46}$ (Kdm5c-fl/fl x Zbtb-Cre)	This manuscript	N/A
Oligonucleotides		
Cre genotyping primers	IDT	Cre Forward: 5'-AGATGCCAGGACATCAGGAACCTG-3' Cre Reverse: 5'-ATCAGCCACACCAGACACAGAGATC-3' Internal control Forward: 5'-CTAGGCCACAGAATTGAAAGATCT-3' Internal control Reverse: 5'-GTAGGTGGAAATTCTAGCATCATCC-3'
Ifnar genotyping primers	IDT	Common Forward: 5'-CGAGGCGAAGTGGTTAAAAG-3' Wild-type Reverse: 5'-ACGGATCAACCTCATTCCAC-3' Mutant Reverse: 5'-AATTCGCCAATGACAAGACG-3'

REAGENT or RESOURCE	SOURCE	IDENTIFIER
Kdm5c genotyping primers	IDT	Forward: 5'-CCATGGAGGCCAGAGAATAAG-3' Reverse: 5'-CTCAGCGGATAAGAGAATTTGCTAC-3'
Kdm5c qPCR primers	IDT	Forward:5'-GAGCAGTCTGTACTGTGCCA-3'; Reverse:5'-ATTCCCACATACAGCCACGG-3'
Software and algorithms		
GraphPad Prism 10	Dotmatrics	https://www.graphpad.com/
FlowJo	FlowJo LLC	https://www.flowjo.com/
Takara's CogentAP v1.5	TaKaRa	https://www.takarabio.com/products/next-generation-sequencing/bioinformatics-tools/cogent-ngs-analysis-pipeline
R v4.1.0	The Comprehensive R Archive Network	https://cran.r-project.org/
DESeq2 v1.32.0	M. I. Love et al.[74]	https://bioconductor.org/packages/release/bioc/html/DESeq2.html
clusterProfiler v4.0.5	G. Yu et al.[75]	https://www.bioconductor.org/packages/release/bioc/html/clusterProfiler.html
TrimGalore v0.6.0	N/A	https://github.com/FelixKrueger/TrimGalore
bwa mem v0.7.17	H. Li[76]	https://github.com/lh3/bwa
SAMBLASTER v0.1.24	G. G. Faust, I. M. Hall[77]	https://github.com/GregoryFaust/samblaster
SAMtools v1.9	H. Li et al.[78]	https://www.htslib.org/
MACS2 v2.2.7.1	Y. Zhang et al.[79]	https://hub.docker.com/r/fooliu/macs2
ENCODE v2 blacklist	H. M. Amemiya et al.[80]	https://github.com/Boyle-Lab/Blacklist
deepTools v3.4.3	F. Ramírez et al.[81]	https://deeptools.readthedocs.io/en/develop/
bamCoverage tool in deepTools	N/A	https://deeptools.readthedocs.io/en/develop/content/tools/bamCoverage.html
WiggleTools v1.2.11	D. R. Zerbino et al.[82]	https://github.com/Ensembl/WiggleTools/releases
DiffBind v3.2.7	C. S. Ross-Innes et al.[83]	https://bioconductor.org/packages/release/bioc/html/DiffBind.html
ChIPSeeker v1.28.3	G. Yu et al.[84]	https://bioconductor.org/packages/release/bioc/html/ChIPseeker.html
pheatmap version 1.0.12 package in R	N/A	https://rdrr.io/cran/pheatmap/
findMotifs.pl script in HOMER version 4.11	S. Heinz et al.[85]	http://homer.ucsd.edu/homer/motif/